

Collaborative and Adaptive Bayesian Optimization for Bounding Variances and Probabilities under Hybrid Uncertainties

Fangqi Hong^a, Pengfei Wei^a, Jingwen Song^{b,*}, Marcos A. Valdebenito^c, Matthias G.R. Faes^c, Michael Beer^{d,e,f}

^a*School of Power and Energy, Northwestern Polytechnical University, Xi'an 710072, China*

^b*School of Mechanical Engineering, Northwestern Polytechnical University, Xi'an 710072, China*

^c*Chair for Reliability Engineering, TU Dortmund University, Leonhard-Euler Strasse 5, 44227, Dortmund, Germany*

^d*Institute for Risk and Reliability, Leibniz Universität Hannover, Hannover 30167, Germany*

^e*Institute for Risk and Uncertainty, University of Liverpool, Liverpool L69 7ZF, UK*

^f*International Joint Research Center for Engineering Reliability and Stochastic Mechanics, Tongji University, Shanghai 200092, China*

Abstract

Uncertainty quantification (UQ) has been widely recognized as of vital importance for reliability-oriented analysis and design of engineering structures, and three groups of mathematical models, i.e., the probability models, the imprecise probability models and the non-probabilistic models, have been developed for characterizing uncertainties of different forms. The propagation of these three groups of models through expensive-to-evaluate simulators to quantify the uncertainties of outputs is then one of the core, yet highly challenging task in reliability engineering, as it involves a demanding double-loop numerical dilemma. For addressing this issue, the Collaborative and Adaptive Bayesian Optimization (CABO) has been developed in our previous work, but it only applies to imprecise probability models and is only capable of bounding the output expectation. We present a substantial improvement of CABO to incorporate all three categories of uncertainty models and to bound arbitrary probabilistic measures such as output variance and failure probability. The algorithm is based on a collaborative active learning mechanism, that is, jointly performing Bayesian optimization in the epistemic uncertainty subspace and Bayesian cubature in the aleatory uncertainty subspace, thus allowing to adaptively produce training samples in the joint uncertainty space. An efficient conditional Gaussian process simulation algorithm is embedded in CABO for acquiring training points and Bayesian inference in both uncertain subspaces. Benchmark studies show that CABO exhibits a remarkable performance in terms of numerical efficiency, accuracy, and global convergence.

Keywords: Uncertainty Quantification; Imprecise Probabilities; Non-probabilistic Model; Bayesian Optimization; Machine Learning; Interval Analysis

1. Introduction

Uncertainty quantification (UQ) is the process of characterizing all sources of uncertainties during numerical simulation of engineering structures, and then quantifying the uncertainties of responses of the simulators, this way to finalize the reliability and/or robustness based analysis and design of the engineering

*Corresponding author at School of Mechanical Engineering, Northwestern Polytechnical University, Xi'an 710072, China
Email address: jingwensong@nwpu.edu.cn (Jingwen Song)

structures. Thus, uncertainty characterization and propagation are the two most important fundamental problems towards this direction. It has been known that alternative types of uncertainties may exist in model parameters, such as properties of material, initial and/or boundary conditions, and environmental excitation [1][2], and it has been demonstrated to be of importance for distinguishing and characterizing different types of uncertainties [3]. Thus, in this section, we briefly review the state-of-the-art scientific understanding and methodological approaches on the categorization, characterization, and propagation of uncertainties presented in engineering simulation, and then present the motivation and main contributions of this work.

Though the sources of uncertainty are diverse, they can be classified into either aleatory or epistemic uncertainty [3][4]. Basically, these two types of uncertainties can be distinguished by judging whether they can be reduced with the enrichment of available information. The aleatory uncertainty, also called stochastic uncertainty or type A uncertainty, is due to the intrinsic randomness of parameters or events, and cannot be reduced with more information. The epistemic uncertainty, also called cognitive uncertainty or type B uncertainty, is reducible as it is caused by the lack of knowledge, and can come from many different sources such as scarcity, incompleteness and imprecision of information. There are three categories of uncertainty characterization models, for characterizing aleatory and epistemic uncertainty: precise probability model, imprecise probability model and non-probability model. For random parameters with sufficient samples, the distribution type and distribution parameters can be inferred precisely, and it is safe to ignore their epistemic uncertainty, the remaining aleatory uncertainty can be characterized by a precise probability model. For random parameters with a lack of information, their distribution type and/or parameters may not be precisely inferred. In this case, both types of uncertainty exist in these parameters and can be separately characterized with imprecise probability models such as probability boxes and evidence theory, see e.g. Refs. [5][6][7][8][9]. For deterministic parameters with a lack of information, their precise values are unknown but known to be crisp, and then only epistemic uncertainty exists, which can be characterized by non-probabilistic models (such as interval and convex models) or subjective probability models [10][11]. Forward propagation of the above three categories of uncertainty characterization models through expensive-to-estimate simulators has been recognized as a vital, yet very challenging numerical task in many areas, and is of concern in this work. Specifically, the joint propagation of the probability model, the probability box model, and the interval model simultaneously is treated in this work.

Uncertainty propagation is a vital branch of uncertainty quantification [12][13], including the estimation of statistical moments [14], distribution function of model response and failure probability [15][16]. The task of this work is to estimate the bounds of the model response variance and structural failure probability given the three types of uncertainty characterization models as inputs. Many state-of-art methods for addressing the above problem involve a double-loop scheme. The most straightforward way to deal with these kinds of problems is to perform global optimization to propagate epistemic uncertainty in the outer loop, and then

for each realization of epistemic parameters in the outer loop, perform a probabilistic analysis in the inner loop [17]. For example, following this approach, Ref. [18] proposed a double-loop scheme to perform global optimization in the outer loop using genetic algorithms and probabilistic analysis in the inner loop using Monte Carlo simulation (MCS). Another double-loop strategy, named as Interval Monte Carlo Simulation (IMCS) [19], performs probabilistic analysis by MCS in the outer loop, and then interval analysis with either intrusive or non-intrusive methods in the inner loop [20][21]. Both double-loop strategies have been successfully applied to the 2014 NASA Langley UQ challenging problem [22]. However, both strategies are known to be inefficient when applied to time-consuming simulators such as finite element models due to the extensive number of required simulator calls, resulting from the double-loop nature.

Decoupling methods provide an efficient way to mitigate the computational cost caused by the double-loop procedure, such as Extended Monte Carlo Simulation (EMCS)[23], Non-intrusive Imprecise Stochastic Simulation (NISS)[12][24] and operator norm theory [25], etc. The EMCS is efficient for propagating imprecise probabilities with low-dimensional epistemic input parameters. The operator norm theory is a theoretically rigorous method capable of decoupling the probabilistic analysis and deterministic simulation and is also proven to be efficient for propagating imprecise stochastic excitation through linear or nonlinear systems [26][27], and has been extended for cases with random and epistemic variables [28]. The NISS is a general methodology framework for propagating imprecise probability models with only one stochastic simulation [12][29][24][30], and equipped with advanced MCS such as subset simulation and line sampling[31], it has been extended to address the rare failure event analysis [29]. The computational cost of all NISS methods is of the same order as the conventional stochastic simulation methods, and thus are efficient. However, when applied to problems with large input epistemic uncertainties, the NISS methods are shown to be less effective especially when the bounds of model response moments and failure probability are of concern.

Surrogate modelling approaches, such as Polynomial chaos expansion [32], neural networks [33], and Gaussian Process Regression (GPR) [34], can be combined with the double-loop methods or decoupling methods, in either an active learning scheme or not, with the aim of generating estimates with acceptable accuracy and decreasing the number of simulator calls. For example, as an improvement of NISS, the Non-intrusive Imprecise Probabilistic Integration (NIPI) has been developed [35], by combining Bayesian inference, the GPR model, and active learning, for improving the performance of NISS when the input epistemic uncertainty is large. However, the method is only applicable to model response expectations and is not suitable for estimating the bounds of probabilistic responses.

An efficient decoupling approach, called Collaborative and Adaptive Bayesian Optimization (CABO), has been developed for estimating the bounds of model response expectation, with few simulator calls [14]. The method jointly performs Bayesian Optimization (BO) and Bayesian Cubature (BC) in an active learning way driven by two distinct acquisition functions, and is shown to own several appealing advantages over

the existing methods. However, the method is currently only applicable to model response expectation, and the case with no interval inputs. The aim of this work is to generalize the method for estimating the bounds of any probabilistic features of responses, with the consideration of all three kinds of input uncertainty characterization models, and specifically, the bounds of model response variance and structural failure probability are of concern. The generalization is realized with an efficient sampling of the GPR model and Monte Carlo estimation of the acquisition functions, and owns all the advantages of the original CABO method, but is of much wider applicability.

The remaining of this work is organized as follows. Section 2 states and analyzes the problems to be addressed, followed by the propositions in section 3, including the review of the basic rationale and simulation of the GPR model, the acquisition functions and their estimations, and the general framework of CABO. Section 4 summarizes the CABO algorithm, and section 5 introduces numerical and engineering examples for illustrating and demonstrating the proposed method, followed by conclusions in section 6.

2. Problem Statements

In this section, we introduce some mathematical concepts, definitions, and mathematical models required for mathematically formulating the uncertainty propagation problems to be solved in this work. Let $y = g(\mathbf{x}_I, \mathbf{x}_{II}, \mathbf{x}_{III})$ denote the response function of the simulator under consideration, where y refers to the scalar model response, $\mathbf{x}_I = (x_I^1, \dots, x_I^{n_I})$ indicates the n_I -dimensional random input vector characterized by a precise probability density function (PDF) $f_I(\mathbf{x}_I)$ and each element is named as a ‘‘Type I variable’’ in the following, $\mathbf{x}_{II} = (x_{II}^1, \dots, x_{II}^{n_{II}})$ implies the n_{II} -dimensional random input vector with hybrid aleatory and epistemic uncertainties modeled by the p-box model $f_{II}(\mathbf{x}_{II} | \boldsymbol{\theta})$ and each of its elements is called a ‘‘Type II variable’’, $\mathbf{x}_{III} = (x_{III}^1, \dots, x_{III}^{n_{III}})$ denotes the n_{III} -dimensional deterministic-but-unknown input vector with the epistemic uncertainty characterized by the hyper-rectangle $[\mathbf{x}_{III}^L, \mathbf{x}_{III}^U]$ and each of its component is called a ‘‘Type III variable’’. In the above setting, the epistemic uncertainty of \mathbf{x}_{II} is associated with the deterministic-but-unknown distribution parameters $\boldsymbol{\theta}$ of dimension n_θ , and is characterized by a hyper-rectangular support $[\boldsymbol{\theta}^L, \boldsymbol{\theta}^U]$. For simplicity, all the three types of input variables are assumed to be independent, and thus the joint PDF of the type I and type II variables can be formulated as $f_I(\mathbf{x}_I) = \prod_{i=1}^{n_I} f_I^i(x_I^i)$ and $f_{II}(\mathbf{x}_{II} | \boldsymbol{\theta}) = \prod_{i=1}^{n_{II}} f_{II}^i(x_{II}^i | \boldsymbol{\theta}^i)$ respectively, with $f_I^i(x_I^i)$ and $f_{II}^i(x_{II}^i | \boldsymbol{\theta}^i)$ indicating the marginal PDFs.

As a summary, the input aleatory uncertainties are characterized by the PDFs $f_I(\mathbf{x}_I)$ and $f_{II}(\mathbf{x}_{II} | \boldsymbol{\theta})$, while the input epistemic uncertainties are modeled by the hyper-rectangles $[\mathbf{x}_{III}^L, \mathbf{x}_{III}^U]$ and $[\boldsymbol{\theta}^L, \boldsymbol{\theta}^U]$. Our target is to develop an efficient method for propagating these three types of uncertainty characterization models through an expensive-to-estimate simulator $g(\mathbf{x}_I, \mathbf{x}_{II}, \mathbf{x}_{III})$, with the specific aim of quantifying the epistemic uncertainties of some probabilistic features of model response y . As the CABO method

has been developed for the model response expectation m_y in our previous work [14], the model output variance V_y and the failure probability p_f are specifically treated in this work. For structural reliability problems, it is assumed that $y < 0$ indicates failure of structure, and then the failure domain is defined as $F = \{(\mathbf{x}_I, \mathbf{x}_{II}, \mathbf{x}_{III}) : g(\mathbf{x}_I, \mathbf{x}_{II}, \mathbf{x}_{III}) < 0\}$. The indicator function of the failure domain is then denoted as $I_F(\mathbf{x}_I, \mathbf{x}_{II}, \mathbf{x}_{III})$ with $I_F(\mathbf{x}_I, \mathbf{x}_{II}, \mathbf{x}_{III}) = 1$ if $(\mathbf{x}_I, \mathbf{x}_{II}, \mathbf{x}_{III}) \in F$ and $I_F(\mathbf{x}_I, \mathbf{x}_{II}, \mathbf{x}_{III}) = 0$ if $(\mathbf{x}_I, \mathbf{x}_{II}, \mathbf{x}_{III}) \notin F$. Given the above setting, both V_y and p_f are functions of the epistemic parameters \mathbf{x}_{III} and $\boldsymbol{\theta}$, and are formulated by integrating out the type I and type II variables as:

$$V_y(\mathbf{x}_{III}, \boldsymbol{\theta}) = \int_{\mathbb{R}^{n_I+n_{II}}} (g(\mathbf{x}_I, \mathbf{x}_{II}, \mathbf{x}_{III}) - m_y(\mathbf{x}_{III}, \boldsymbol{\theta}))^2 f_I(\mathbf{x}_I) f_{II}(\mathbf{x}_{II}|\boldsymbol{\theta}) d\mathbf{x}_I d\mathbf{x}_{II} \quad (1)$$

and

$$p_f(\mathbf{x}_{III}, \boldsymbol{\theta}) = \int_{\mathbb{R}^{n_I+n_{II}}} I_F(\mathbf{x}_I, \mathbf{x}_{II}, \mathbf{x}_{III}) f_I(\mathbf{x}_I) f_{II}(\mathbf{x}_{II}|\boldsymbol{\theta}) d\mathbf{x}_I d\mathbf{x}_{II} \quad (2)$$

respectively, where

$$m_y(\mathbf{x}_{III}, \boldsymbol{\theta}) = \int_{\mathbb{R}^{n_I+n_{II}}} g(\mathbf{x}_I, \mathbf{x}_{II}, \mathbf{x}_{III}) f_I(\mathbf{x}_I) f_{II}(\mathbf{x}_{II}|\boldsymbol{\theta}) d\mathbf{x}_I d\mathbf{x}_{II} \quad (3)$$

indicates the response expectation function. The bounds of variance and probability of failure can then be formulated as:

$$\begin{cases} V_L = \min_{\boldsymbol{\theta} \in [\boldsymbol{\theta}^L, \boldsymbol{\theta}^U], \mathbf{x}_{III} \in [\mathbf{x}_{III}^L, \mathbf{x}_{III}^U]} V_y(\mathbf{x}_{III}, \boldsymbol{\theta}) \\ V_U = \max_{\boldsymbol{\theta} \in [\boldsymbol{\theta}^L, \boldsymbol{\theta}^U], \mathbf{x}_{III} \in [\mathbf{x}_{III}^L, \mathbf{x}_{III}^U]} V_y(\mathbf{x}_{III}, \boldsymbol{\theta}) \end{cases} \quad (4)$$

and

$$\begin{cases} p_{fL} = \min_{\boldsymbol{\theta} \in [\boldsymbol{\theta}^L, \boldsymbol{\theta}^U], \mathbf{x}_{III} \in [\mathbf{x}_{III}^L, \mathbf{x}_{III}^U]} p_f(\mathbf{x}_{III}, \boldsymbol{\theta}) \\ p_{fU} = \max_{\boldsymbol{\theta} \in [\boldsymbol{\theta}^L, \boldsymbol{\theta}^U], \mathbf{x}_{III} \in [\mathbf{x}_{III}^L, \mathbf{x}_{III}^U]} p_f(\mathbf{x}_{III}, \boldsymbol{\theta}) \end{cases} \quad (5)$$

The most straightforward way for addressing the above problems commonly involves a double-loop procedure, which is time-consuming for expensive-to-evaluate simulators. To overcome this challenge, in what follows we develop the CABO algorithm with the combination of BO and BC in a collaborative scheme.

3. Collaborative and Adaptive Bayesian Optimization: rationale and key procedures

The aim of this section is to introduce the theoretical framework of the CABO algorithm for bounding the response variance and the failure probability, and then present some key developments for enriching and realizing this algorithm framework. Thus, subsection 3.1 presents the theoretical rationale of the CABO algorithm, and then highlights the necessities of sampling from the stochastic processes for approximating

$V_y(\mathbf{x}_{III}, \boldsymbol{\theta})$ and $p_f(\mathbf{x}_{III}, \boldsymbol{\theta})$, following which, the training and sampling strategies are developed in subsection 3.2. Then, the procedure of BO performed in the subspace of epistemic uncertainty, and the procedure of BC performed in the subspace of aleatory uncertainty are presented in subsections 3.3 and 3.4 respectively.

3.1. The CABO framework

The CABO algorithm is developed based on two Bayesian numerical analysis methods [36], i.e., BO [37] and BC [38][39], with the GPR model serving as a surrogate model of the model simulator. The Bayesian numerical analysis is a cutting-edge direction for addressing nearly all kinds of challenging numerical tasks such as cubature, optimization, solving ODE/PDE and structural reliability analysis, and has received extensive attention recently [40]. Compared with traditional numerical methods, the Bayesian approaches have many advantages; precisely, the two most appealing features are the involved active learning schemes and the Bayesian inference strategies. In this context, the former feature allows the algorithm to achieve acceptable estimates with much less simulator calls. Also, the latter feature allows to generate measures of numerical errors of the estimates, which guarantees the convergence to some extent. As it will be seen in what follows, the combination of BO and BC for solving the Eq. (4) and Eq. (5) retains the above two features. In the CABO framework, these two Bayesian numerical algorithms are implemented in a collaborative and adaptive way, realizing the decoupling of the two loops, thus the algorithm is named CABO.

As can be seen from Eq. (4) and Eq. (5), estimating the bounds of response variance and failure probability involves numerical optimization in the outer loop for searching the global optima of \mathbf{x}_{III} and $\boldsymbol{\theta}$, as well as numerical cubature in the inner loop to estimate the values of the variance and failure probability given fixed values of \mathbf{x}_{III} and $\boldsymbol{\theta}$. This typical double-loop scheme makes the required number of simulator calls tremendously large, which is commonly unacceptable in real-world applications. Inspired by the above process, the CABO is devised and involves the following key steps: 1) training a GPR model with an initial design point set \mathbf{D} in the augmented space of aleatory variables (\mathbf{x}_I and \mathbf{x}_{II}) and epistemic parameters (\mathbf{x}_{III} and $\boldsymbol{\theta}$); 2) performing BO equipped with a proper acquisition function in the marginal space of the epistemic parameters to achieve a new design site $(\mathbf{x}_{III}^+, \boldsymbol{\theta}^+)$, with the principle of improving the optimization solution quality the most; 3) for fixed point $(\mathbf{x}_{III}^+, \boldsymbol{\theta}^+)$, performing BC equipped with another proper acquisition function in the marginal space of aleatory variables (e.g., the subspace of \mathbf{x}_I and \mathbf{x}_{II}) to identify a new design point $(\mathbf{x}_I^+, \mathbf{x}_{II}^+)$, with the principle of improving the cubature accuracy the most; 4) the simulator is then called at the joint design point $(\mathbf{x}_I^+, \mathbf{x}_{II}^+, \mathbf{x}_{III}^+, \boldsymbol{\theta}^+)$ to enrich the training data set \mathbf{D} ; 5) the algorithm ends only if stopping criteria for both BO and BC are satisfied. The above CABO framework is schematically shown in Figure 1.

As mentioned above, the GPR model for Bayesian inference is trained in the augmented space of $(\mathbf{x}_I, \mathbf{x}_{II}, \mathbf{x}_{III}, \boldsymbol{\theta})$, however, the simulator function is defined in the marginal space of the three types of

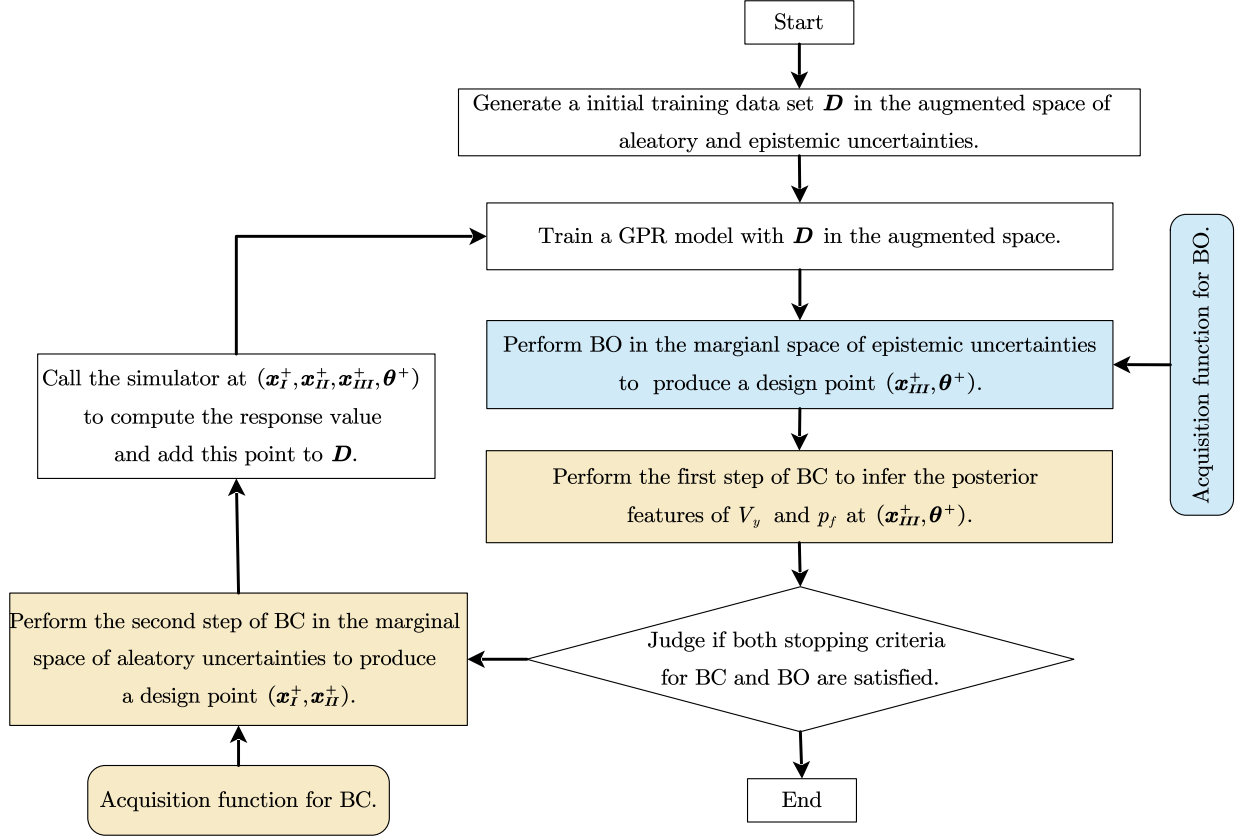


Figure 1: The CABO framework.

variables $(\mathbf{x}_I, \mathbf{x}_{II}, \mathbf{x}_{III})$, and does not explicitly depend on θ . To fill this gap, a probabilistic transformation needs to be implemented before implementing CABO. As the type II variables are independent of each other, we take the individual type II variable x_{II}^i as an example. Let $\mathbf{u}_{II} = (u_{II}^1, \dots, u_{II}^{n_{II}})$ with each element being a random variable uniformly distributed in $[0, 1]$. Let $F_{II}^i(x_{II}^i|\theta^i)$ denote the cumulative distribution function of x_{II}^i , which is assumed to be continuous. Then, it is known that this CDF admits uniform distribution in $[0, 1]$ whatever distribution type does x_{II}^i follow. Thus, let $u_{II}^i = F_{II}^i(x_{II}^i|\theta^i)$, the inverse transformation can be formulated as $x_{II}^i = F_{II}^{i-1}(u_{II}^i|\theta^i)$. For the input vector \mathbf{x}_{II} , denote the transformation as $\mathbf{x}_{II} = T(\mathbf{u}_{II}|\theta)$ for simplicity, then a modified simulator function can be obtained as $\mathcal{G}(\omega) = g(\mathbf{x}_I, T(\mathbf{u}_{II}|\theta), \mathbf{x}_{III})$, where $\omega = (\mathbf{x}_I, \mathbf{u}_{II}, \mathbf{x}_{III}, \theta)$.

It is now clear that the key elements of the CABO framework include training a GPR model for approximating $\mathcal{G}(\omega)$ in the augmented space, performing BO in the marginal space of epistemic uncertainties, and implementing BC in the marginal space of aleatory uncertainties, etc. Besides, to make the CABO applicable to arbitrary probabilistic responses of interest (such as response variance and failure probability concerned in this work), it is necessary to introduce an efficient sampling procedure for simulating the GPR

model. In the following, all the above key elements will be introduced.

3.2. Gaussian process regression and sampling strategy

Assume that $\hat{\mathcal{G}}(\boldsymbol{\omega})$ follows a Gaussian process denoted as $\mathcal{GP}(m(\boldsymbol{\omega}), \kappa(\boldsymbol{\omega}, \boldsymbol{\omega}'))$, with $m(\boldsymbol{\omega})$ and $\kappa(\boldsymbol{\omega}, \boldsymbol{\omega}')$ being the prior mean function and the prior covariance function respectively. The mean function can be set as zero, constant or polynomial functions, and the covariance function (also named as kernel function) measures the correlation of $\hat{\mathcal{G}}(\boldsymbol{\omega})$ at any two sites $\boldsymbol{\omega}$ and $\boldsymbol{\omega}'$. The choice of the covariance function depends on the properties (e.g., smoothness, stationarity) of $\mathcal{G}(\boldsymbol{\omega})$, and one can refer to e.g., chapter 4 of Ref.[34] for details. Without loss of generality, the exponential squared kernel function, which is applicable for smooth functions, is utilized as an example in this paper, which is formulated as:

$$\kappa(\boldsymbol{\omega}, \boldsymbol{\omega}') = \sigma_0^2 \exp\left(-\frac{1}{2}(\boldsymbol{\omega} - \boldsymbol{\omega}')^\top \Sigma^{-1}(\boldsymbol{\omega} - \boldsymbol{\omega}')\right), \quad (6)$$

where σ_0^2 and Σ represent the hyper-parameters of the covariance function. One should note the proposed CABO algorithm applies whatever kernel function is utilized.

Let $\mathbf{D} = (\mathbf{W}, \mathbf{Y})$ indicate the training data set of size N_0 , where \mathbf{W} refers to the sample matrix with N_0 rows, whose i -th row refers to the i -th sample of $\boldsymbol{\omega}$, and $\mathbf{Y} = \mathcal{G}(\mathbf{W})$. Based on the prior assumptions on $\hat{\mathcal{G}}(\boldsymbol{\omega})$, the column vector \mathbf{Y} follows a N_0 -dimensional Gaussian distribution. Taking the N_0 -dimensional joint probability density function as the likelihood function, which is formulated as:

$$\mathcal{L}(\mathbf{D}) = \frac{1}{(2\pi)^{(N_0)/2} |\mathbf{K}|^{1/2}} \exp\left(-\frac{1}{2}(\mathbf{Y} - \mathbf{m}(\mathbf{W}))^\top \mathbf{K}^{-1}(\mathbf{Y} - \mathbf{m}(\mathbf{W}))\right), \quad (7)$$

where $\mathbf{K} = \kappa(\mathbf{W}, \mathbf{W})$ denotes a $N_0 \times N_0$ matrix with the (i, j) -th component K_{ij} being $\kappa(\mathbf{W}_i, \mathbf{W}_j)$, and \mathbf{W}_i is the i -th row of \mathbf{W} . By minimizing the negative logarithm of $\mathcal{L}(\mathbf{D})$, the hyper-parameters involved in the prior mean and covariance functions can be identified [34].

With all hyper-parameters estimated, the posterior Gaussian process $\hat{\mathcal{G}}_{\mathbf{D}}(\mu_y(\boldsymbol{\omega}), \text{COV}_y(\boldsymbol{\omega}, \boldsymbol{\omega}'))$ can be derived, whose mean, variance and covariance are formulated as:

$$\mu_y(\boldsymbol{\omega}) = m(\boldsymbol{\omega}) + \boldsymbol{\kappa}(\mathbf{W}, \boldsymbol{\omega})^\top \mathbf{K}^{-1}(\mathbf{Y} - \mathbf{m}(\mathbf{W})), \quad (8)$$

,

$$\sigma_y^2(\boldsymbol{\omega}) = \sigma_0^2 - \boldsymbol{\kappa}(\mathbf{W}, \boldsymbol{\omega})^\top \mathbf{K}^{-1} \boldsymbol{\kappa}(\mathbf{W}, \boldsymbol{\omega}), \quad (9)$$

and

$$\text{COV}_y(\boldsymbol{\omega}, \boldsymbol{\omega}') = \kappa(\boldsymbol{\omega}, \boldsymbol{\omega}') - \boldsymbol{\kappa}(\mathbf{W}, \boldsymbol{\omega})^\top \mathbf{K}^{-1} \boldsymbol{\kappa}(\mathbf{W}, \boldsymbol{\omega}') \quad (10)$$

respectively, where $\boldsymbol{\kappa}(\mathbf{W}, \boldsymbol{\omega})$ is a N_0 -dimensional column vector, the i -th component of which is $\kappa(\mathbf{W}_i, \boldsymbol{\omega})$.

It should be noted that the posterior mean $\mu_y(\boldsymbol{\omega})$ refers to the mean prediction at any site $\boldsymbol{\omega}$, while the posterior variance $\sigma_y^2(\boldsymbol{\omega})$ measures the prediction error at $\boldsymbol{\omega}$.

Once the GPR model $\hat{\mathcal{G}}_{\mathcal{D}}(\boldsymbol{\omega})$ is trained, according to Eq. (1) and Eq. (2), the variance and failure probability are functions of the GPR model $\hat{\mathcal{G}}_{\mathcal{D}}(\boldsymbol{\omega})$ and thus, are also stochastic processes and denoted by $\hat{\mathcal{V}}_y(\mathbf{x}_{III}, \boldsymbol{\theta})$ and $\hat{\mathcal{P}}_f(\mathbf{x}_{III}, \boldsymbol{\theta})$ respectively. For proceeding with the proposed methods, a sampling scheme for generating random samples of the stochastic process $\hat{\mathcal{V}}_y(\mathbf{x}_{III}, \boldsymbol{\theta})$ and $\hat{\mathcal{P}}_f(\mathbf{x}_{III}, \boldsymbol{\theta})$ is required. However, it is difficult to directly sample from $\hat{\mathcal{V}}_y$ and $\hat{\mathcal{P}}_f$ as the distribution type of stochastic process and the distribution parameters cannot be explicitly known. Alternatively, an indirect strategy is introduced here for numerically estimating the samples for both $\hat{\mathcal{V}}_y$ and $\hat{\mathcal{P}}_f$ based on the samples generated from the posterior GPR model. An efficient sampling procedure, named as ‘‘GPR conditioning sampling scheme’’, developed in [41] is applied to sample from the posterior GPR model $\hat{\mathcal{G}}_{\mathcal{D}}(\boldsymbol{\omega})$. Assume that $\hat{h}_{\mathcal{D}}(\boldsymbol{\omega})$ follows an unconditional Gaussian process $\mathcal{GP}(0, \kappa(\boldsymbol{\omega}, \boldsymbol{\omega}'))$, define an auxiliary GP model $\hat{\mathcal{H}}_{\mathcal{D}}(\boldsymbol{\omega})$ as:

$$\hat{\mathcal{H}}_{\mathcal{D}}(\boldsymbol{\omega}) = \mu_y(\boldsymbol{\omega}) - \hat{\mu}_y(\boldsymbol{\omega}) + \hat{h}_{\mathcal{D}}(\boldsymbol{\omega}) \quad (11)$$

with $\hat{\mu}_y(\boldsymbol{\omega})$ being

$$\hat{\mu}_y(\boldsymbol{\omega}) = m(\boldsymbol{\omega}) + \boldsymbol{\kappa}(\mathbf{W}, \boldsymbol{\omega})^{\text{T}} \mathbf{K}^{-1} \left(\hat{h}_{\mathcal{D}}(\mathbf{W}) - m(\mathbf{W}) \right). \quad (12)$$

It was concluded in Ref. [41] that $\hat{\mathcal{H}}_{\mathcal{D}}(\boldsymbol{\omega})$ admits exactly the same probability distribution as the Gaussian process $\hat{\mathcal{G}}_{\mathcal{D}}(\boldsymbol{\omega})$, meaning that the samples of $\hat{\mathcal{G}}_{\mathcal{D}}(\boldsymbol{\omega})$ can be obtained by simulating $\hat{\mathcal{H}}_{\mathcal{D}}(\boldsymbol{\omega})$. Moreover, it can deduced by Eq. (11) that the samples of $\hat{\mathcal{G}}_{\mathcal{D}}(\boldsymbol{\omega})$ can be simply gained by sampling from the unconditional GP model $\hat{h}_{\mathcal{D}}(\boldsymbol{\omega})$.

There are many ways to sample from the unconditional GP model $\hat{h}_{\mathcal{D}}(\boldsymbol{\omega})$ for producing the samples $\hat{\mathcal{G}}_{\mathcal{D}}^{(j)}(\boldsymbol{\omega})$ with $j = 1, \dots, N_g$, such as, the expansion optimal linear estimation method (EOLE) [42], Karhunen–Lo eve (KL) expansion [43], stochastic harmonic function representation (SHFR) [44], Sparse GP-based simulation [45][46], etc. In this paper, the KL expansion is employed to draw N_g samples of the random field. These samples comprise N_{cut} independently standard Gaussian variables, where, N_{cut} represents the truncation terms determined by the accuracy of eigenvalues and eigenfunctions derived from eigen-decomposition of covariance function of GP model [47]. Moreover, by numerically estimating the eigen-pairs, continuous samples of GP model can be generated with one expansion [34].

With all the above considerations, the following procedure is applied to evaluate the variance and failure probability as cast in Eqs. (1) and (2). Generate a set of joint samples $\mathbf{W} = (\mathbf{X}_I, \mathbf{U}_{II}, \mathbf{X}_{III}, \mathbf{T})$ of size N_x . Once the sample set $\hat{\mathcal{G}}_{\mathcal{D}}^{(j)}(\boldsymbol{\omega})$ of the posterior Gaussian process $\hat{\mathcal{G}}_{\mathcal{D}}(\boldsymbol{\omega})$ is obtained, the samples $\hat{\mathcal{V}}_y^{(j)}$

and $\hat{\mathcal{P}}_f^{(j)}$ of the stochastic process $\hat{\mathcal{V}}_y(\mathbf{x}_{III}, \boldsymbol{\theta})$ and $\hat{\mathcal{P}}_f(\mathbf{x}_{III}, \boldsymbol{\theta})$ can be deduced as:

$$\hat{\mathcal{V}}_y^{(j)}(\mathbf{x}_{III}, \boldsymbol{\theta}) = \frac{1}{N_x - 1} \sum_{i=1}^{N_x} \left[\hat{\mathcal{G}}_D^{(j)}(\mathbf{X}_I^{(i)}, \mathbf{U}_{II}^{(i)}, \mathbf{x}_{III}, \boldsymbol{\theta}) - \frac{1}{N_x} \sum_{k=1}^{N_x} \hat{\mathcal{G}}_D^{(j)}(\mathbf{X}_I^{(k)}, \mathbf{U}_{II}^{(k)}, \mathbf{x}_{III}, \boldsymbol{\theta}) \right]^2 \quad (13)$$

and

$$\hat{\mathcal{P}}_f^{(j)}(\mathbf{x}_{III}, \boldsymbol{\theta}) = \frac{1}{N_x} \sum_{i=1}^{N_x} \left[\hat{\mathcal{G}}_D^{(j)}(\mathbf{X}_I^{(i)}, \mathbf{U}_{II}^{(i)}, \mathbf{x}_{III}, \boldsymbol{\theta}) < 0 \right] \quad (14)$$

with $\mathbf{X}_I^{(i)}$ and $\mathbf{U}_{II}^{(i)}$ being the i -th row of \mathbf{X}_I and \mathbf{U}_{II} respectively. The corresponding mean function $\mu_V(\mathbf{x}_{III}, \boldsymbol{\theta})$ and variance function $\sigma_V^2(\mathbf{x}_{III}, \boldsymbol{\theta})$ of $\hat{\mathcal{V}}_y$ can be evaluated as:

$$\begin{cases} \hat{\mu}_V(\mathbf{x}_{III}, \boldsymbol{\theta}) = \frac{1}{N_g} \sum_{j=1}^{N_g} \hat{\mathcal{V}}_y^{(j)}(\mathbf{x}_{III}, \boldsymbol{\theta}) \\ \hat{\sigma}_V^2(\mathbf{x}_{III}, \boldsymbol{\theta}) = \frac{1}{N_g - 1} \sum_{j=1}^{N_g} \left[\hat{\mathcal{V}}_y^{(j)}(\mathbf{x}_{III}, \boldsymbol{\theta}) - \mu_V(\mathbf{x}_{III}, \boldsymbol{\theta}) \right]^2 \end{cases}, \quad (15)$$

and for $\hat{\mathcal{P}}_f(\mathbf{x}_{III}, \boldsymbol{\theta})$, the mean function $\mu_{p_f}(\mathbf{x}_{III}, \boldsymbol{\theta})$ and variance function $\sigma_{p_f}^2(\mathbf{x}_{III}, \boldsymbol{\theta})$ are approximated by

$$\begin{cases} \hat{\mu}_{p_f}(\mathbf{x}_{III}, \boldsymbol{\theta}) = \frac{1}{N_g} \sum_{j=1}^{N_g} \hat{\mathcal{P}}_f^{(j)}(\mathbf{x}_{III}, \boldsymbol{\theta}) \\ \hat{\sigma}_{p_f}^2(\mathbf{x}_{III}, \boldsymbol{\theta}) = \frac{1}{N_g - 1} \sum_{j=1}^{N_g} \left[\hat{\mathcal{P}}_f^{(j)}(\mathbf{x}_{III}, \boldsymbol{\theta}) - \mu_{p_f}(\mathbf{x}_{III}, \boldsymbol{\theta}) \right]^2 \end{cases}. \quad (16)$$

One should note that, the above MCS estimators will converge to the true values as the sample size approaches infinity. The posterior means given by Eqs. (15) and (16) can be seen as the mean predictions of response variance and failure probability at any site $(\mathbf{x}_{III}, \boldsymbol{\theta})$, and the corresponding posterior variances measure the corresponding prediction errors.

For illustrating the above sampling strategy, we take a simple numerical example with model function $g(\mathbf{x}) = x_1 (\cos(\pi x_2) + 1) + x_2$ as an example, where x_1 follows standard normal distribution and x_2 is an interval variable with support $[0, 2]$. With this setting, both the model response variance and the failure probability depend on the epistemic parameter x_2 . A training sample set of size 15 is randomly generated and used for training the GPR model, and then one hundred functional samples are generated for the posterior GPR model based on the above ‘‘GPR conditioning sampling scheme’’. With Eq. (13) and (14), each of these functional samples results in a functional sample for $V_y(x_2)$ and $p_f(x_2)$, as shown in Figure 2, together with the true functions $V_y(x_2)$ and $p_f(x_2)$ for comparison. It is shown that these functional samples show variations, adapted from the variation of the GPR model. Although the probability distribution of $\hat{\mathcal{V}}_y$ and $\hat{\mathcal{P}}_f$ cannot be precisely known, these function samples do provide sufficient information for performing BO in the subspace of epistemic uncertainties.

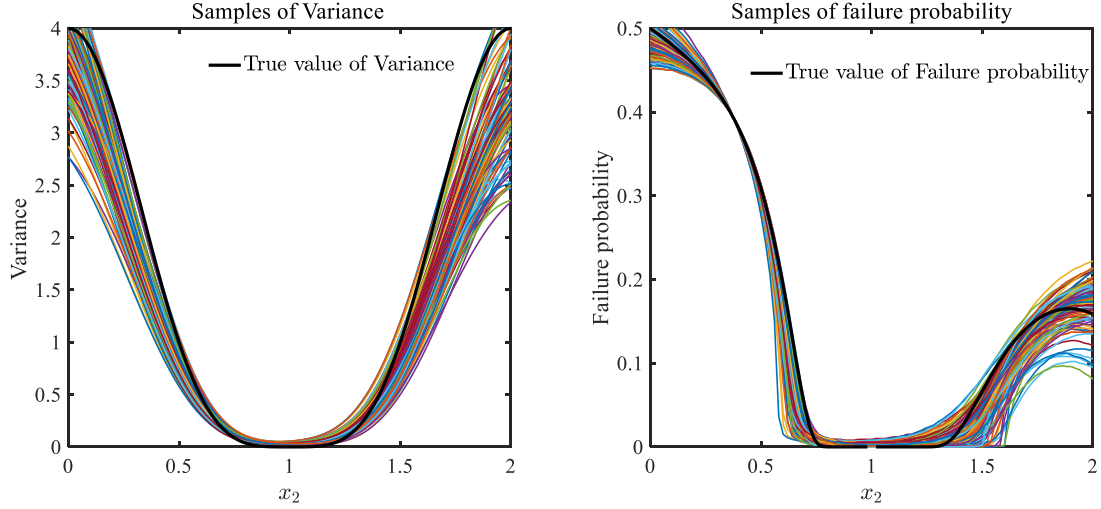


Figure 2: An example of generating random samples for the stochastic processes $\hat{V}_y(x_2)$ and $\hat{p}_f(x_2)$, and the corresponding true functional curves of $V_y(x_2)$ and $p_f(x_2)$ are also given for comparison.

3.3. Bayesian optimization in subspace of epistemic uncertainties

BO is a typical Bayesian numerical analysis method. It is based on surrogating the objective function with the GPR model, and then inferring the most plausible global optima and the next training point which results in the best improvement for inferring the global optima. The core of a BO algorithm is the acquisition function, which is responsible for identifying the best design points. Many acquisitions have been developed for BO, such as the Probability of Improvement (PI) function [48], the Expected Improvement (EI) function [49], the knowledge-gradient (KG) function [50], and the entropy search (ES) function [51]. Of this approaches, the EI function is the most popular one as it admits a closed-form expression when the objective function is approximated with the GPR model. Many variants of the EI function have also been developed for better balancing global exploration and local exploitation. In this work, we extend the EI function for searching the global optima of both $\hat{V}_y(\mathbf{x}_{III}, \boldsymbol{\theta})$ and $\hat{P}_f(\mathbf{x}_{III}, \boldsymbol{\theta})$ where the surrogate models do not follow a Gaussian distribution. Without loss of generality, the EI functions for the lower bounds of the response variance function and the failure probability function are formulated as:

$$\mathcal{L}_V^{\text{BO}}(\mathbf{x}_{III}, \boldsymbol{\theta}) = \mathbb{E}_{\mathcal{D}} \left[\max \left(\mu_V(\mathbf{x}_{III}^*, \boldsymbol{\theta}^*) - \hat{V}_y(\mathbf{x}_{III}, \boldsymbol{\theta}), 0 \right) \right] \quad (17)$$

and

$$\mathcal{L}_{p_f}^{\text{BO}}(\mathbf{x}_{III}, \boldsymbol{\theta}) = \mathbb{E}_{\mathcal{D}} \left[\max \left(\mu_{p_f}(\mathbf{x}_{III}^*, \boldsymbol{\theta}^*) - \hat{P}_f(\mathbf{x}_{III}, \boldsymbol{\theta}), 0 \right) \right], \quad (18)$$

respectively, where $\mathbb{E}_{\mathcal{D}}[\cdot]$ refers to the expectation operator taken over the Gaussian process $\hat{\mathcal{G}}_{\mathcal{D}}(\boldsymbol{\omega})$.

In Eqs. (17) and (18), $\mu_V(\mathbf{x}_{III}, \boldsymbol{\theta})$ and $\mu_{p_f}(\mathbf{x}_{III}, \boldsymbol{\theta})$ denote the posterior means of the response variance function and the failure probability function respectively, and $(\mathbf{x}_{III}^*, \boldsymbol{\theta}^*)$ represents the current best guess

of the global optimum point, which can be obtained by the following equation

$$(\mathbf{x}_{III}^*, \boldsymbol{\theta}^*) = \arg \min \mu_V(\mathbf{x}_{III}, \boldsymbol{\theta}) + \alpha \sigma_V(\mathbf{x}_{III}, \boldsymbol{\theta}) \quad (19)$$

and

$$(\mathbf{x}_{III}^*, \boldsymbol{\theta}^*) = \arg \min \mu_{p_f}(\mathbf{x}_{III}, \boldsymbol{\theta}) + \alpha \sigma_{p_f}(\mathbf{x}_{III}, \boldsymbol{\theta}), \quad (20)$$

where α denotes the degree of risk aversion, which is set to be 1 in this work. For saving computational cost, the solutions of Eq. (19) and Eq. (20) are found in the training data set \mathbf{D} . The theoretical explanation of the EI function is given as follows. Consider the estimation of the failure probability as an example. The quantity $\max(\mu_{p_f}(\mathbf{x}_{III}^*, \boldsymbol{\theta}^*) - \hat{\mathcal{P}}_f(\mathbf{x}_{III}, \boldsymbol{\theta}), 0)$ measures the amount of reduction of the failure probability function value at $(\mathbf{x}_{III}, \boldsymbol{\theta})$ compared to the current best guess $(\mathbf{x}_{III}^*, \boldsymbol{\theta}^*)$, and this quantity is a random variable due to the randomness of the stochastic process $\hat{\mathcal{P}}_f(\mathbf{x}_{III}, \boldsymbol{\theta})$. The EI function defined by Eq. (18) is then explained as the expected reduction of the failure probability value at $(\mathbf{x}_{III}, \boldsymbol{\theta})$ compared to the current best guess, and by observing the point with the highest EI value and adding it to the training data to update the GPR model and then the induced stochastic process $\hat{\mathcal{P}}_f(\mathbf{x}_{III}, \boldsymbol{\theta})$, the next best guess of the global minimum point can be inferred.

The next issue of concern is to compute the global maximum point of the EI functions. Unfortunately, both Eq. (17) and Eq. (18) do not admit closed-form expressions since the probability distribution of $\hat{\mathcal{V}}_y$ and $\hat{\mathcal{P}}_f$ cannot be explicitly known. We propose to compute the two functions with MCS based on the random samples of $\hat{\mathcal{V}}_y$ and $\hat{\mathcal{P}}_f$ generated with the sampling strategy developed in the last subsection. Specifically, the Monte Carlo estimators for the two EI functions are formulated as:

$$\begin{cases} \hat{\mathcal{L}}_V^{\text{BO}}(\mathbf{x}_{III}, \boldsymbol{\theta}) = \frac{1}{N_g} \sum_{j=1}^{N_g} \max(\hat{\mu}_V(\mathbf{x}_{III}^*, \boldsymbol{\theta}^*) - \hat{\mathcal{V}}_y^{(j)}(\mathbf{x}_{III}, \boldsymbol{\theta}), 0) \\ \hat{\mathcal{L}}_{p_f}^{\text{BO}}(\mathbf{x}_{III}, \boldsymbol{\theta}) = \frac{1}{N_g} \sum_{j=1}^{N_g} \max(\hat{\mu}_{p_f}(\mathbf{x}_{III}^*, \boldsymbol{\theta}^*) - \hat{\mathcal{P}}_f^{(j)}(\mathbf{x}_{III}, \boldsymbol{\theta}), 0) \end{cases}. \quad (21)$$

By maximizing Eq. (21), a new design site $(\mathbf{x}_{III}^+, \boldsymbol{\theta}^+)$ can be solved, i.e.,

$$(\mathbf{x}_{III}^+, \boldsymbol{\theta}^+) = \arg \max \hat{\mathcal{L}}_V^{\text{BO}}(\mathbf{x}_{III}, \boldsymbol{\theta}) \quad (22)$$

or

$$(\mathbf{x}_{III}^+, \boldsymbol{\theta}^+) = \arg \max \hat{\mathcal{L}}_{p_f}^{\text{BO}}(\mathbf{x}_{III}, \boldsymbol{\theta}). \quad (23)$$

The objective functions of the above two optimization problems are cheap to estimate, and thus many global optimization algorithms can be used for efficiently finding the solutions. In this work, the Particle Swarm

Optimization (PSO) is suggested. The stopping criterion for BO can be defined as:

$$\mathcal{L}^{\text{BO}}(\mathbf{x}_{III}^+, \boldsymbol{\theta}^+) < \Delta^{\text{BO}} \quad (24)$$

or

$$\frac{\mathcal{L}^{\text{BO}}(\mathbf{x}_{III}^+, \boldsymbol{\theta}^+)}{\left(\max_{\boldsymbol{\omega} \in \mathcal{D}} \hat{\mathcal{V}}_y(\mathbf{x}_{III}, \boldsymbol{\theta}) - \min_{\boldsymbol{\omega} \in \mathcal{D}} \hat{\mathcal{V}}_y(\mathbf{x}_{III}, \boldsymbol{\theta})\right)} < \Delta^{\text{BO}} \quad (25)$$

$$\frac{\mathcal{L}^{\text{BO}}(\mathbf{x}_{III}^+, \boldsymbol{\theta}^+)}{\left(\max_{\boldsymbol{\omega} \in \mathcal{D}} \hat{\mathcal{P}}_f(\mathbf{x}_{III}, \boldsymbol{\theta}) - \min_{\boldsymbol{\omega} \in \mathcal{D}} \hat{\mathcal{P}}_f(\mathbf{x}_{III}, \boldsymbol{\theta})\right)} < \Delta^{\text{BO}}$$

, where Δ^{BO} is specified by the users selected from $10^{-3} - 10^{-2}$.

3.4. Bayesian cubature in subspace of aleatory uncertainties

By maximizing the EI acquisition function introduced in subsection 3.3, the next design site $(\mathbf{x}_{III}^+, \boldsymbol{\theta}^+)$ in the marginal space of epistemic uncertainty is identified. In this subsection, the joint identification of the training point $(\mathbf{x}_I^+, \mathbf{u}_{II}^+)$ in the aleatory subspace is of interest, such that this point reduces the posterior variances of predictions. One notes the acquisition functions for the two quantities are in totally different form, as the one for response variance seeks to reduce the numerical error of the simulator function over the full support of the aleatory variables, while the one for failure probability aims at improving the accuracy of the failure boundary. In what follows, the Posterior Variance Contribution (PVC) acquisition function for response variance, and the U acquisition function for failure probability are respectively introduced.

3.4.1. Posterior variance contribution function for response variance

The PVC function is originally developed by some of the authors in Ref.[52] for active design of training points for BC where the integrand is approximated by a GPR model. However, in Ref.[53], the PVC function is also shown to be effective for computation of the response variance and variance-based sensitivity indices. Thus, the PVC function is utilized here for the response variance. Mathematically, the PVC function is defined as:

$$\mathcal{L}^{\text{PVC}}(\mathbf{x}_I, \mathbf{u}_{II}) = f_I(\mathbf{x}_I) f_u(\mathbf{u}_{II}) \int_{\mathbb{R}^{n_I+n_{II}}} \text{cov}_y((\mathbf{x}_I, \mathbf{u}_{II}, \mathbf{x}_{III}^+, \boldsymbol{\theta}^+), (\mathbf{x}'_I, \mathbf{u}'_{II}, \mathbf{x}_{III}^+, \boldsymbol{\theta}^+)) f_I(\mathbf{x}'_I) f_u(\mathbf{u}'_{II}) d\mathbf{x}'_I d\mathbf{u}'_{II}, \quad (26)$$

where $f_u(\mathbf{u}_{II})$ is the density function of the uniform probability distribution with unit support $[0, 1]$. It can be easily proved that the PVC function formulated in Eq. (26) has the following property,

$$\sigma_{\hat{m}_y}^2(\mathbf{x}_{III}^+, \boldsymbol{\theta}^+) = \int_{\mathbb{R}^{n_I+n_{II}}} \mathcal{L}^{\text{PVC}}(\mathbf{x}_I, \mathbf{u}_{II}) f_I(\mathbf{x}_I) f_u(\mathbf{u}_{II}) d\mathbf{x}_I d\mathbf{u}_{II}, \quad (27)$$

where, the variance $\sigma_{\hat{m}_y}^2(\mathbf{x}_{III}^+, \boldsymbol{\theta}^+)$ denotes the predict error of the response expectation function formulated in Eq. (3). As can be seen from Eq. (26) and (27), the value of PVC function measures the contribution of the prediction uncertainty at the site $(\mathbf{x}_I, \mathbf{u}_{II})$ to the posterior variance of $\hat{m}_y(\mathbf{x}_{III}^+, \boldsymbol{\theta}^+)$ with the consideration of the spatial correlation of this site with all the others over the marginal space of the aleatory uncertainties. By adding the maximum point of the PVC function, denoted as $(\mathbf{x}_I^+, \mathbf{u}_{II}^+)$, jointly with the design site $(\mathbf{x}_{III}^+, \boldsymbol{\theta}^+)$, to the training data for updating the GPR model, it is expected to reduce the prediction errors of the model response expectation and variance the most, one can refer to Ref. [52] for more details. Consider a simple numerical example, the posterior distribution of the GPR model is shown in the first panel of Figure 3, the corresponding PVC function is displayed in the second panel. With the maximum point of the PVC function added to the training data set, the updated posterior information is given in the third panel of Figure 3. As it can be seen, the posterior variance has been reduced to a large extent, indicating that the accuracy of posterior mean function for replacing the true g -function has been greatly improved.

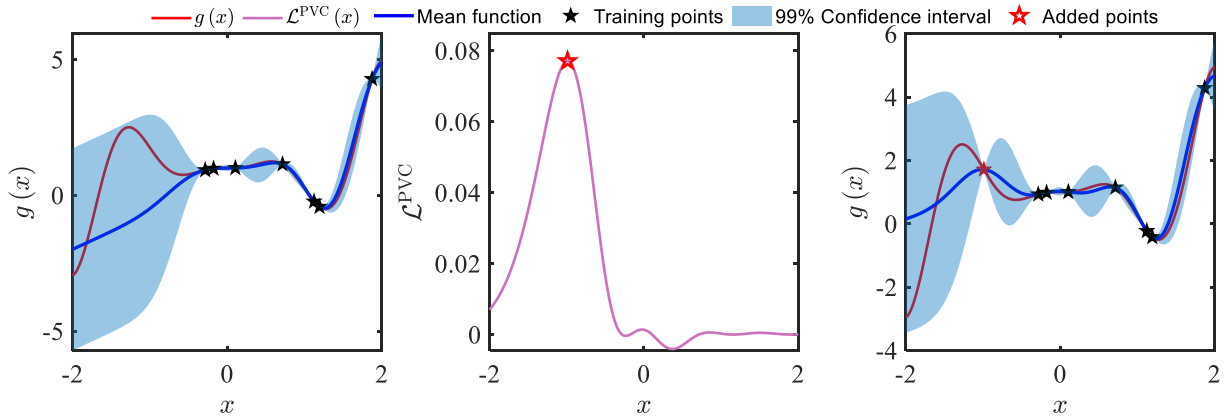


Figure 3: The illustration of PVC function for a simple numerical example.

As that the closed-form expressions of the PVC function are available for specific pairs of probability density function and kernel function [38], we propose to compute the PVC function value by MCS. Given the joint samples $\mathbf{W} = (\mathbf{X}_I, \mathbf{U}_{II}, \mathbf{X}_{III}, \mathbf{T})$ of size N_x , the Monte Carlo estimator of the PVC function is formulated as:

$$\hat{\mathcal{L}}^{\text{PVC}}(\mathbf{x}_I, \mathbf{u}_{II}) = f_I(\mathbf{x}_I) \times f_u(\mathbf{u}_{II}) \times \frac{1}{N_x} \sum_{i=1}^{N_x} \text{cov}_y \left((\mathbf{x}_I, \mathbf{u}_{II}, \mathbf{x}_{III}^+, \boldsymbol{\theta}^+), (\mathbf{X}_I^{(i)}, \mathbf{U}_{II}^{(i)}, \mathbf{x}_{III}^+, \boldsymbol{\theta}^+) \right). \quad (28)$$

The next design site $(\mathbf{x}_I^+, \mathbf{u}_{II}^+)$ is then generated by computing the maximum point of Eq. (28), and similarly, the PSO algorithm is suggested as the PVC function is very cheap to compute.

With the above collaborative design strategy, a design site $\boldsymbol{\omega}^+ = (\mathbf{x}_I^+, \mathbf{u}_{II}^+, \mathbf{x}_{III}^+, \boldsymbol{\theta}^+)$ is then obtained in the augmented space of aleatory and epistemic uncertainties. By adding this point to the training data set,

not only the knowledge on the global optimum point can improved to a large extent, but also the estimation accuracy of the response variance at this point can be largely enhanced. For each iteration, we need only to call the simulator for one time, making the method approach the true solution in a high convergence speed. The stopping condition of $\hat{\mathcal{L}}^{\text{PVC}}(\mathbf{x}_I, \mathbf{u}_{II})$ is set as:

$$\text{COV}_V(\mathbf{x}_{III}^+, \boldsymbol{\theta}^+) = \frac{\sqrt{\hat{\sigma}_V^2(\mathbf{x}_{III}^+, \boldsymbol{\theta}^+)}}{\hat{\mu}_V(\mathbf{x}_{III}^+, \boldsymbol{\theta}^+)} < \Delta^{\text{PVC}}, \quad (29)$$

where $\text{COV}_V(\mathbf{x}_{III}^+, \boldsymbol{\theta}^+)$ denotes the Coefficient Of Variation (COV) of response variance, Δ^{PVC} denotes the stopping threshold, which, based on our experience, can be any value between 0.01 and 0.05, depending on the users' tolerance on numerical error. The value of $\text{COV}_V(\mathbf{x}_{III}^+, \boldsymbol{\theta}^+)$ represents the normalized error of the mean prediction $\hat{\mu}_V(\mathbf{x}_{III}^+, \boldsymbol{\theta}^+)$. The lower the value of $\text{COV}_V(\mathbf{x}_{III}^+, \boldsymbol{\theta}^+)$ is, the more precise the estimate $\hat{\mu}_V(\mathbf{x}_{III}^+, \boldsymbol{\theta}^+)$ is. In this context, it is assumed that the estimate $\hat{\mu}_V(\mathbf{x}_{III}^+, \boldsymbol{\theta}^+)$ is precise when $\text{COV}_V(\mathbf{x}_{III}^+, \boldsymbol{\theta}^+)$ is less than Δ^{PVC} .

The above collaborative active learning procedure is repeated until both the stopping condition for BO in Eq. (24) and the one for BC in Eq. (29) are satisfied. It is then known that the knowledge on the lower bound of model response can no longer be improved, both the global minimum point as well as the response variance value at this point are accurately computed.

3.4.2. U function for failure probability

Similarly, many acquisition functions for failure probability estimation have been developed, for example, the U function [54], the expected feasibility function [55], the H function [56], and the expected integrated error reduction function [39], where the U function is the mostly well-known, and thus is utilized in this work. The U function is defined as:

$$U(\mathbf{x}_I, \mathbf{u}_{II}) = \frac{|\hat{\mu}_y(\mathbf{x}_I, \mathbf{u}_{II}, \mathbf{x}_{III}^+, \boldsymbol{\theta}^+)|}{\hat{\sigma}_y(\mathbf{x}_I, \mathbf{u}_{II}, \mathbf{x}_{III}^+, \boldsymbol{\theta}^+)}. \quad (30)$$

The value of $\Phi(-U(\mathbf{x}_I, \mathbf{u}_{II}))$ measures the probability of misjudging the sign of $\mathcal{G}(\mathbf{x}_I, \mathbf{u}_{II}, \mathbf{x}_{III}^+, \boldsymbol{\theta}^+)$. Thus, with the minimum point of $U(\mathbf{x}_I, \mathbf{u}_{II})$ added to the training set, the estimate of failure probability will be more accurate. Search the minimum point $(\mathbf{x}_I^+, \mathbf{u}_{II}^+)$ in the given joint samples set $\mathbf{W} = (\mathbf{X}_I, \mathbf{U}_{II}, \mathbf{X}_{III}, \mathbf{T})$, i.e.,

$$(\mathbf{x}_I^+, \mathbf{u}_{II}^+) = \arg \min_{(\mathbf{x}_I, \mathbf{u}_{II}) \in (\mathbf{X}_I, \mathbf{U}_{II})} U(\mathbf{x}_I, \mathbf{u}_{II}). \quad (31)$$

The stopping criteria is formulated as:

$$\text{COV}_{p_f}(\mathbf{x}_{III}^+, \boldsymbol{\theta}^+) = \frac{\sqrt{\hat{\sigma}_{p_f}^2(\mathbf{x}_{III}^+, \boldsymbol{\theta}^+)}}{\hat{\mu}_{p_f}(\mathbf{x}_{III}^+, \boldsymbol{\theta}^+)} < \Delta^{\text{U}}, \quad (32)$$

where $\text{COV}_{p_f}(\mathbf{x}_{III}^+, \boldsymbol{\theta}^+)$ denotes the posterior COV of the failure probability estimate, and Δ^U indicates the stopping threshold, which is usually chosen within the range $[0.01, 0.05]$.

Once the pair $(\mathbf{x}_I^+, \mathbf{u}_{II}^+)$ being identified, add $\boldsymbol{\omega}^+ = (\mathbf{x}_I^+, \mathbf{u}_{II}^+, \mathbf{x}_{III}^+, \boldsymbol{\theta}^+)$ and $y^+ = \mathcal{G}(\boldsymbol{\omega}^+)$ to the training data set and update the GPR model, until Eq. (24) and Eq. (32) are satisfied simultaneously. Similar to the case for response variance, the above CABO procedure for estimating the bounds of failure probability requires only one simulator call for each iteration. Benefiting from the global convergence of the BO algorithms, the CABO algorithm is expected to have good performance on global convergence.

4. Collaborative and Adaptive Bayesian Optimization: algorithms

Based on the theoretical developments given in Section 3, the aim of this section is to present the detailed CABO algorithms for bounding the response variance (in subsection 4.1) and the failure probability (in subsection 4.2).

4.1. Bounds of response variance

With all the developments in section 3, the pseudocode of CABO for estimating the lower bound of the response variance is summarized in Algorithm 1. The algorithm can be easily extended for computing the upper bound by setting the training data generated for computing the lower bound as the initial training data, and modifying the EI function as the one for upper bound estimation. Therefore, additional details for locating the upper bound are omitted.

Before implementing Algorithm 1, some algorithm parameters, including the sample size N_x of \mathbf{W} , the sample size N_g of the GPR model, the stopping thresholds Δ^{BO} and Δ^{PVC} , need to be pre-specified. The value of N_x needs to be specified such that the COV of the estimator for each of the response variance sample $\hat{\mathcal{Y}}_y^{(j)}$ is less than a threshold, and this parameter can also be adaptively adjusted if the implementation process to adaptively meet the above requirement. Based on the experience, setting N_x as several thousands meets the requirement for most examples. The value of N_g is set based on the principle that the COVs of the estimators for all acquisition functions and variance response terms need to be less than a threshold, and based on numerical experience, setting N_g as a value between 10^3 and 5×10^3 is a reasonable choice. The settings for the two stopping thresholds has been reported in subsection 3.3 and 3.4 respectively.

It should be noted that, although Algorithm 1 is specifically developed for estimating the lower bound of the response variance, it also applies to the upper bound computation, and the bounds of any order of

moments of model response.

Algorithm 1: CABO method for estimating the bounds of response variance

Input: Augmented g -function $\mathcal{G}(\mathbf{W})$, sample size N_x, N_g, N_0 , stopping threshold $\Delta^{\text{BO}}, \Delta^{\text{COV}}$

Output: Bounds of response variance and its corresponding sites.

- 1 Generate a set of joint samples $\mathbf{W} = (\mathbf{X}_I, \mathbf{U}_{II}, \mathbf{X}_{III}, \mathbf{T})$ of size N_x by random sampling;
- 2 Create the initial training set \mathbf{D} of size N_0 by random sampling from \mathbf{W} , let $N_{\text{call}} = N_0$;
- 3 **while** $(1 = 1)$ **do**
- 4 Train or update the GPR model $\hat{\mathcal{G}}_{\mathbf{D}}(\boldsymbol{\omega})$ based on training data set \mathbf{D} ;
- 5 Generate a set of N_g samples $\hat{\mathcal{G}}_{\mathbf{D}}^{(j)}(\boldsymbol{\omega})$ for $\hat{\mathcal{G}}_{\mathbf{D}}(\boldsymbol{\omega})$ with $j = 1, \dots, N_g$ by using the GPR conditioning sampling scheme introduced in subsection 3.2;
- 6 Find the current best solution $(\mathbf{x}_{III}^*, \boldsymbol{\theta}^*)$ by solving Eq. (19) in \mathbf{D} ;
- 7 Compute the design site $(\mathbf{x}_{III}^+, \boldsymbol{\theta}^+)$ by Eq. (22);
- 8 Evaluate the response variance $\hat{\mu}_V(\mathbf{x}_{III}^+, \boldsymbol{\theta}^+)$ by utilizing Eq. (15);
- 9 Compute the design site $(\mathbf{x}_I^+, \mathbf{u}_{II}^+)$ by maximizing Eq. (28);
- 10 **if** both Eq. (24) and Eq. (29) are satisfied **then**
- 11 | break **while-do**;
- 12 **else**
- 13 | Compute the value of $\mathcal{G}(\boldsymbol{\omega}^+)$ by calling the simulator, where $\boldsymbol{\omega}^+ = (\mathbf{x}_I^+, \mathbf{u}_{II}^+, \mathbf{x}_{III}^+, \boldsymbol{\theta}^+)$, and let $N_{\text{call}} = N_{\text{call}} + 1$;
- 14 | Add $(\boldsymbol{\omega}^+, \mathcal{G}(\boldsymbol{\omega}^+))$ to the training data set \mathbf{D} ;
- 15 **end**
- 16 **end**
- 17 Output the minimum $\hat{\mu}_V(\mathbf{x}_{III}^+, \boldsymbol{\theta}^+)$ of response variance, and minimum point $(\mathbf{x}_I^+, \mathbf{u}_{II}^+, \mathbf{x}_{III}^+, \boldsymbol{\theta}^+)$.

4.2. Bounds of failure probability

Using the EI function formulated in Eq. (21) for BO and U function given in Eq. (30) for BC, the pseudocode of CABO for estimating the lower bound of the failure probability is described as Algorithm 2. For the upper bound, one can easily make the extension thus, details are omitted. This algorithm is also applicable for estimating the bounds of CDF of the model response.

The settings of sample size N_x of \mathbf{W} , the sample size N_g of the GPR model, the stopping thresholds Δ^{BO} and Δ^{U} involved in Algorithm 2 follow the same principles as Algorithm 1. The value of N_x can be set to be $100/p_f$ for making the COV of each failure probability sample $\hat{\mathcal{P}}_f^{(j)}$ less than a given threshold. The value of N_g is recommended to be chosen from interval $[1000, 5000]$ such that the COVs of the estimators for all acquisition functions and failure probability terms are less than a threshold. The values of two stopping thresholds Δ^{BO} and Δ^{U} are proposed in subsection 3.3 and 3.4 respectively. It should be noted

that the upper bound gets more attention among the bounds of failure probability in practical engineering application. For precisely and efficiently estimating the bound of failure probability (less than 10^{-3}), subset simulation, line sampling, etc, can be integrated to CABO, which is not the focus of this work.

Algorithm 2: CABO method for estimating the bounds of failure probability

Input: Augmented g -function $\mathcal{G}(\mathbf{W})$, sample size N_x, N_g, N_0 , stopping threshold $\Delta^{\text{BO}}, \Delta^{\text{COV}}$

Output: Bounds of variance and its corresponding sites.

- 1 Generate a set of joint samples $\mathbf{W} = (\mathbf{X}_I, \mathbf{U}_{II}, \mathbf{X}_{III}, \mathbf{T})$ of size N_x by random sampling;
- 2 Create the initial training set \mathbf{D} of size N_0 from sample pool \mathbf{W} , let $N_{\text{call}} = N_0$;
- 3 **while** $(1 = 1)$ **do**
 - 4 Train or update the GPR model $\hat{\mathcal{G}}_{\mathbf{D}}(\boldsymbol{\omega})$ based on training set \mathbf{D} ;
 - 5 Generate a set of N_g samples $\hat{\mathcal{G}}_{\mathbf{D}}^{(j)}(\boldsymbol{\omega})$ for $\hat{\mathcal{G}}_{\mathbf{D}}(\boldsymbol{\omega})$ with $j = 1, \dots, N_g$;
 - 6 Find the current best solution $(\mathbf{x}_{III}^*, \boldsymbol{\theta}^*)$ by solving Eq. (20) in \mathbf{D} ;
 - 7 Compute the design site $(\mathbf{x}_{III}^+, \boldsymbol{\theta}^+)$ by Eq. (23);
 - 8 Evaluate the response variance $\hat{\mu}_{p_f}(\mathbf{x}_{III}^+, \boldsymbol{\theta}^+)$ by utilizing Eq. (16);
 - 9 Compute the design site $(\mathbf{x}_I^+, \mathbf{u}_{II}^+)$ by solving Eq. (31);
 - 10 **if** both Eq. (24) and Eq. (32) are satisfied **then**
 - 11 | break **while-do**;
 - 12 **else**
 - 13 | Compute the value of $\mathcal{G}(\boldsymbol{\omega}^+)$ by calling the simulator, where $\boldsymbol{\omega}^+ = (\mathbf{x}_I^+, \mathbf{u}_{II}^+, \mathbf{x}_{III}^+, \boldsymbol{\theta}^+)$, and let $N_{\text{call}} = N_{\text{call}} + 1$;
 - 14 | Add $(\boldsymbol{\omega}^+, \mathcal{G}(\boldsymbol{\omega}^+))$ to the training data set \mathbf{D} ;
 - 15 **end**
- 16 **end**
- 17 Output the minimum $\mu_{p_f}(\mathbf{x}_{III}^+, \boldsymbol{\theta}^+)$ of variance, and minimum point $(\mathbf{x}_I^+, \mathbf{u}_{II}^+, \mathbf{x}_{III}^+, \boldsymbol{\theta}^+)$.

5. Benchmark studies

In this section, we present one numerical example to illustrate the implementations details and demonstrate the feasibility of the CABO algorithm for bounding both the response variance and the failure probability given the three types of uncertainty characterization models as inputs, and then introduce three engineering examples across distinct disciplines to demonstrate the wide applicability of the CABO method to real-world engineering problems.

5.1. An numerical illustrative example

For illustrating the effectiveness of the proposed method for estimating the bounds of response variance and failure probability, two numerical examples are utilized respectively, and the corresponding model

functions are formulated as:

$$g_1(\mathbf{x}) = x_1(x_2^2 + x_2 + \cos(\pi x_3) - 7) \quad (33)$$

and

$$g_2(\mathbf{x}) = 7 - (x_1 + x_3)^2 + x_2. \quad (34)$$

For g_1 -function, x_1 follows standard normal distribution, x_2 follows the normal distribution $N(\mu, 2)$, with $\mu \in [-1.3, 1.8]$, and x_3 is a interval variable supported by $[-0.5, 1.3]$. For g_2 -function, x_1 follows standard normal distribution $N(0, 1)$, x_2 is a random variable modeled by the normal p-box $N(\mu, 2)$ with $\mu \in [-2, 1]$, and x_3 is a deterministic-but-unknown variable with the epistemic uncertainty characterized by the interval $[-1, 2]$.

We perform the CABO method to estimate the bounds of variance of g_1 -function by setting the initial training size N_0 to be 30, the sample size N_x of \mathbf{W} to be 10000, the sample size N_g of the GPR model to be 1000, Δ^{BO} to be 0.005, and Δ^{PVC} to be 0.01. The results of CABO are displayed in Figure 4 and Table 1, together with the reference computed analytically for comparison. For this implementation, the CABO consumes 35 simulator calls for estimating the lower bound, and then 20 more simulator calls for estimating the upper bounds. Thus, the total number of simulator calls for estimating both bounds is 85. As can be seen From Figure 4, as the stopping conditions are satisfied, the CABO algorithms has successfully reached the global optimal points where the bounds of response variance locate, demonstrating the accuracy and convergence of CABO for this problem. Comparing the ultimate results of CABO and the reference solutions summarized in Table 1, it is found that both the locations and values of each bound computed by CABO match well with the reference solutions, and the Posterior COVs of estimates for both bounds are sufficiently small, indicating that the CABO algorithms converges to the global optima with high accuracy and numerical robustness.

Table 1: Results for the bounds of response variance of the numerical illustrative example with simulator function g_1 .

Method	Bounds	Means	Optima of (x_3, μ)	Posterior COVs (%)	N_{call}
Reference	Lower	19	(0, 1.3028)	-	-
	Upper	54.563	(1, -0.5)	-	
CABO	Lower	18.980	(0.05, 1.26)	0.06	30+35+20=85
	Upper	54.627	(1.0207, -5726)	0.01	

Then, the bounds of failure probability of g_2 -function is evaluated by the CABO algorithm with $N_0 = 12$, $N_x = 10000$, $N_g = 1000$, $\Delta^{\text{BO}} = 0.005$, and $\Delta^{\text{U}} = 0.01$, the corresponding results are displayed in Figure 5 and Table 2, where the reference values are evaluated by a double-loop scheme, where the PSO is performed in the outer loop for optimization and the MCS with 100000 samples is implemented in the inner loop for estimating the failure probability values. The training details of CABO in the subspace of epistemic uncertainty shown in Figure 5 reveal that the proposed CABO has successfully converged to the global

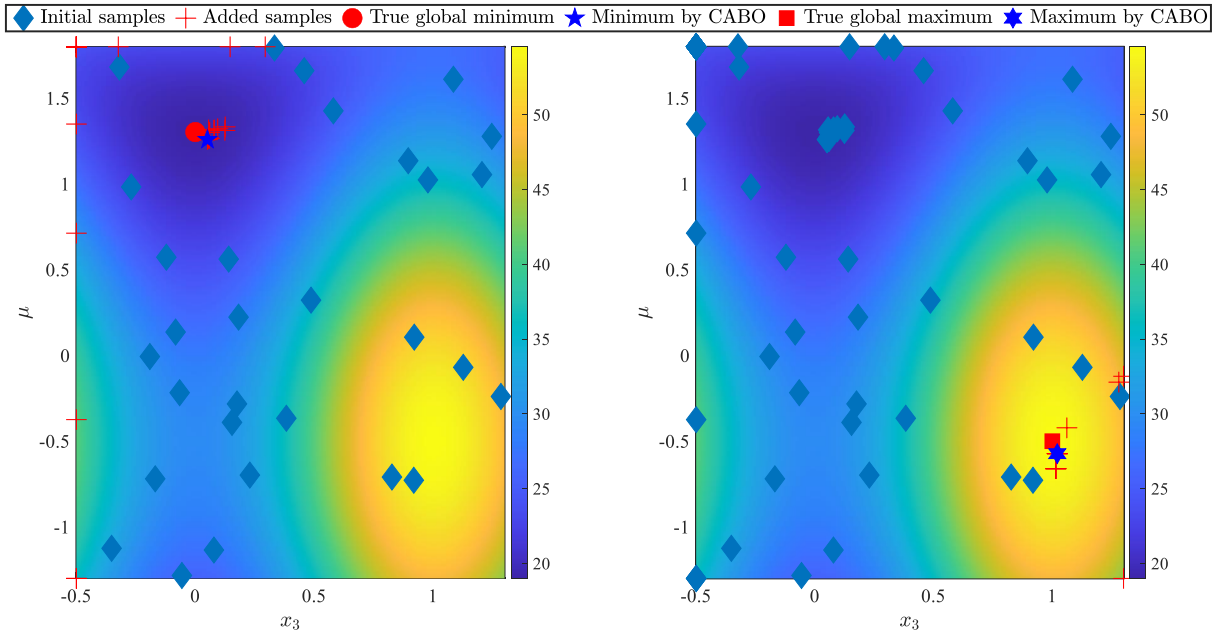


Figure 4: Training details of CABO in the epistemic subspace for estimating the lower bound (left) and upper bound (right) for the numerical illustrative example with simulator function g_1 , where the heat maps refer to the reference solution of the response variance function $V(x_3, \mu)$.

optima for both lower and upper bounds. The results reported in Table 2 indicate that both bounds of failure probability are accurately estimated with CABO as the values match well with the reference solutions and the Posterior COVs are sufficiently small. It is also shown that the posterior COV of the lower bound is obviously higher than that of the upper bound, and this is due to the fact that the lower bound of failure probability is significantly smaller than the upper bound, resulted from the large epistemic uncertainties of inputs. It is shown in Table 1 that this phenomenon also appears for the response variance.

Table 2: Results for the bounds of response variance of the numerical illustrative example with simulator function g_2 .

Method	Bounds	Means	Optima of (x_3, μ)	Posterior COVs (%)	N_{call}
Reference	Lower	0.0071	(-0.0264, 1)	–	–
	Upper	0.4296	(2, -2)	–	–
CABO	Lower	0.0076	(-0.0353, 1)	0.50	12+13+4=29
	Upper	0.4203	(2, -2)	0.04	

5.2. Application to a spacecraft control system

We then apply the proposed CABO algorithm to the pitch control system of a spacecraft with its body modeled as rigid body. The problem is adapted from Ref. [57]. Ignoring the inertance of the engine swing

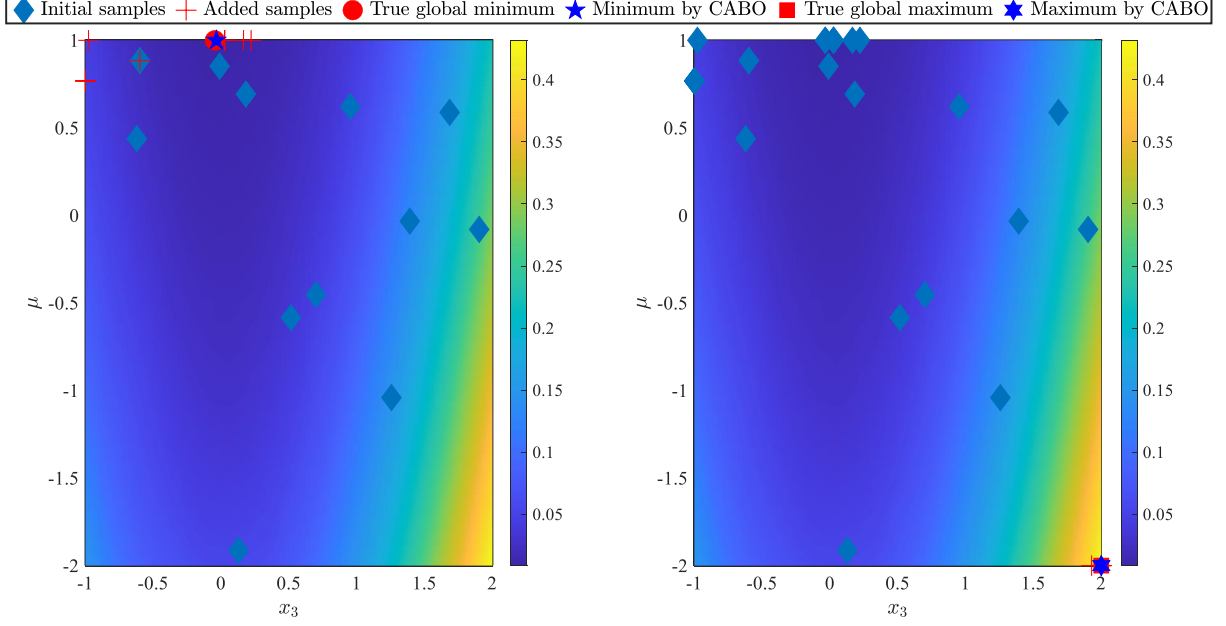


Figure 5: Training details in interval space of x_3 and μ of CABO for evaluating the bounds of failure probability for the illustrative example with model function g_2 , where the heat maps refer to the reference solution of the failure probability function $p_f(x_3, \mu)$.

tube, the linearized motion control function is formulated as:

$$\begin{aligned}
 \Delta \dot{\theta} &= (c_2 - c_1) \theta + c_1 \Delta \varphi + c_3 \delta_\varphi + \bar{F}_y \\
 \Delta \dot{\omega}_z &= b_2 \Delta \theta - b_2 \Delta \varphi - b_1 \Delta \omega_z - b_3 \delta_\varphi + \bar{M}_z \\
 \Delta \dot{\phi} &= \Delta \omega_z
 \end{aligned} \tag{35}$$

with $\Delta \theta$, $\Delta \omega_z$, $\Delta \phi$ and δ_φ being the speed dip, pitch rate, pitch angle, and the equivalent swing angle of tail nozzle respectively, the rigid body coefficients are expressed as:

$$\begin{aligned}
 c_1 &= \frac{P + C_L^\alpha q S}{mV}, c_2 = \frac{g \sin \theta}{V}, c_3 = \frac{P}{mV} \\
 b_1 &= -\frac{C_{m_z}^{\omega_z} q S L^2}{J_z V}, b_2 = -\frac{C_{m_z}^\alpha q S L}{J_z}, b_3 = \frac{C_{m_z}^{\delta_z} q S L}{J_z}
 \end{aligned} \tag{36}$$

where P , V , q , S , L , m and J_z denote the engine thrust, the spacecraft speed, the dynamic pressure, the reference area, the reference length, the mass and the moment of inertia respectively, all of the above parameters are set to be constant. The aeronautic parameters are represented by C_L^α , $C_{m_z}^{\omega_z}$, $C_{m_z}^\alpha$ and $C_{m_z}^{\delta_z}$, their detailed information is displayed in Table 3. Following the notations given in section 2, $x_I = C_L^\alpha$, $x_{II} = (C_{m_z}^{\omega_z}, C_{m_z}^\alpha)$, $x_{III} = C_{m_z}^{\delta_z}$, and $\boldsymbol{\theta} = (\mu_1, \mu_2, \sigma_1, \sigma_2)$.

Table 3: The information of the pneumatic parameter of the space control.

Parameters	Distribution type	Means	Std	Ranges
C_L^α	Beta	6.4013	0.3201	[5.4411, 7.3615]
$C_{mz}^{\omega z}$	Beta	$\mu_1 \in [-0.11, -0.09]$	$\sigma_1 \in [0.0045, 0.0055]$	[-0.1150, -0.0850]
C_{mz}^α	Beta	$\mu_2 \in [-0.30, -0.25]$	$\sigma_2 \in [0.0125, 0.0150]$	[-0.3290, -0.2432]
$C_{mz}^{\delta z}$	-	-	-	[-0.3211, -0.2373]

Based on the above equations of motion, the spacecraft rigid body transfer function is formulated as:

$$W_b = -\frac{b_3s + (b_3c_1 - b_2c_1 - b_3c_2)}{s^3 + (b_1 - c_2 + c_1)s^2 + (b_1c_1 - b_1c_2 + b_2)s - b_2c_2}. \quad (37)$$

The dynamic characteristics of the servo system of the engine oscillation are replaced by the inertia link approximation, and the corresponding transfer function is given by

$$W_{sf} = \frac{1}{T_c s + 1} \quad (38)$$

, where T_c represents the time constant of the servo system. The feedback Proportional plus Derivative (PD) controller is applied as the control methods, and the transfer function of which is formulated as:

$$W_c = (a_0 + a_1s) \quad (39)$$

where a_0 and a_1 denote the static and dynamic gain respectively. In summary, the open loop transfer function of the whole control system can be given by

$$W = W_{sf}W_bW_c \quad (40)$$

The concern for the control system is whether it can remain stable under disturbances and commands, and achieve reasonable dynamic performance on this basis. In the frequency domain, the limit state function concerning the amplitude margin is a function of $\mathbf{x} = (C_L^\alpha, C_{mz}^{\omega z}, C_{mz}^\alpha, C_{mz}^{\delta z})$, and defined as:

$$g(\mathbf{x}) = 12 - L_c(\mathbf{x}) \quad (41)$$

, where $L_c(\mathbf{x}) = 20 \lg |W(j\omega_g)|$ represents the amplitude margin with $W(j\omega_g)$ being the cut frequency. Next we use CABO to estimate the bounds of variance and failure probability of g -function.

To estimate the bounds of response variance, the algorithm parameters of CABO are set as follows. The initial training data size N_0 is set to be 30, the sample size N_x of \mathbf{W} is set to be 10000, the sample size N_g of the GPR model is set to be 1000, the stopping thresholds Δ^{BO} and Δ^{COV} are set to be 0.01 and 0.02 respectively. The results are summarized in Table 4. The reference solutions are computed with the

double-loop procedure, where the PSO is implemented in the outer loop for estimating the bounds, and the MCS based on 10^4 samples is utilized in the inner loop for computing the values of response variance. As can be seen, both the optima and the bound values computed by CABO are in good agreement with the reference solutions, and the posterior COVs of both bounds are sufficiently small. The above facts indicate that the CABO results are accurate and robust.

Then, the CABO method is also utilized to estimate the bounds of failure probability. The parameters of CABO are selected as $N_0 = 30$, $N_x = 10^4$, $N_g = 10^3$, $\Delta^{\text{BO}} = 0.01$, and $\Delta^{\text{U}} = 0.02$. The results of CABO and the reference one are displayed in Table 5, where the reference results are obtained by utilizing the same double-loop scheme as above. As can be seen, the bounds of failure probability estimated by CABO show no difference with the reference values and the corresponding COVs are very small. Based on the above results, it can be demonstrated that the CABO method can efficiently and accurately estimate the bounds of failure probability. The differences between the optimal points obtained by CABO and reference points are somewhat large as revealed in Table 4 and Table 5, it is probably because the sensitivities of the response variance to some pneumatic parameters are lower in the area around the extreme point or there are multiple extreme points in the whole epistemic space.

Table 4: Results of response variance bounds for the spacecraft control system.

Method	Bounds	Means	Optima of $(x_{III}, \boldsymbol{\theta})$	Posterior COVs (%)	N_{call}
Reference	Lower	0.3026	(0.2373, 0.11, 0.3, 0.0045, 0.0125)	–	–
	Upper	0.4118	(0.3211, 0.09, 0.2551, 0.0055, 0.0150)	–	–
CABO	Lower	0.3052	(0.2373, 0.11, 0.2812, 0.0053, 0.0125)	0.001	30+14+2=46
	Upper	0.4439	(0.2373, 0.11, 0.2930, 0.0055, 0.0150)	0.17	

Table 5: Results of failure probability bounds for the spacecraft control system.

Method	Bounds	Means	Optima of $(x_{III}, \boldsymbol{\theta})$	Posterior COVs (%)	N_{call}
Reference	Lower	0	(0.2851, 0.0914, 0.2533, 0.0052, 0.0126)	–	–
	Upper	0.0565	(0.2373, 0.11, 0.3, 0.0048, 0.015)	–	–
CABO	Lower	0	(0.2547, 0.1051, 0.2525, 0.005, 0.0147)	–	30+0+11=41
	Upper	0.0545	(0.2373, 0.11, 0.3, 0.0055, 0.015)	1.09	

5.3. Transmission tower

Consider a electricity transmission tower utilized in the power grid system, the structure of the tower is shown in Figure 6, one can refer [31] and [58] to for details. The Finite Element (FE) model of the transmission tower is build and solved with Matlab. Eighty bars make up the tower, the properties of all bars are linear elastic, four dynamic loads are applied to the tower at the top nodes displayed in Figure 6. The young's modulus $E_1^c - E_4^c$ and the cross-section $A_1^c - A_4^c$ of four of the corner are assumed to be random variables, the distributional information of $E_1^c - E_4^c$ and $A_1^c - A_4^c$ are reported in Table 6. Let $\boldsymbol{x} = (E_1^c, \dots, E_4^c, A_1^c, \dots, A_4^c)$ be the 8-dimensional input variables. Following the notations in section 2 and the assumption in Table 6, it

can be known that the random variables consists of $\mathbf{x}_I = (E_1^c, E_2^c)$ and $\mathbf{x}_{II} = (E_3^c, E_4^c)$, while the epistemic parameters include $\mathbf{x}_{III} = (A_1^c, A_2^c, A_3^c, A_4^c)$ and $\boldsymbol{\theta} = (\mu_{E3}, \mu_{E4}, \sigma_{E3}, \sigma_{E4})$. Assume that when the displacement of node A denoted by d_A exceeds 0.0432, the structure of the transmission tower failures, then, the limit state function can be formulated as:

$$g(\mathbf{x}) = 0.0432 - d_A(\mathbf{x}) \quad (42)$$

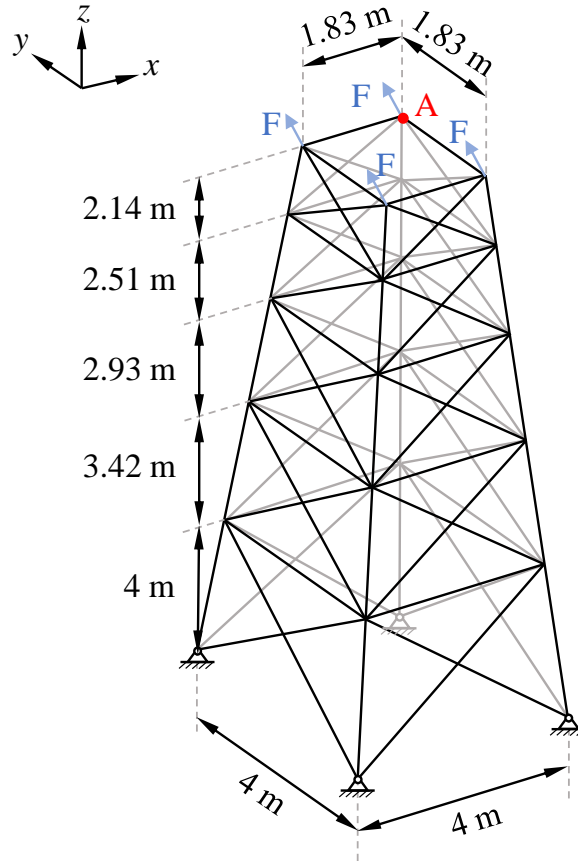


Figure 6: The geometric structure and environmental condition of the transmission tower.

Before performing the CABO method to evaluate the bounds of response variance, the parameters involved in CABO are need to be assigned. Let N_0 be 35, N_x be 10000, N_g be 1000, Δ^{BO} be 0.01, and Δ^{PVC} be 0.02. The results are given in Table 7. The reference results are evaluated by a double-loop procedure as described above. As it can be seen, both of bounds and optimal points estimated by CABO show good consistency with the reference values and the corresponding posterior COVs are quite small.

For the case of calculating the bounds of probability of failure, we initialize the parameters N_0 , N_x , N_g , Δ^{BO} and Δ^{U} included in CABO be 30, 10000, 1000, 0.01 and 0.02 respectively. The results of CABO

Table 6: The distributional information of the transmission tower.

Parameters	Distribution type	Means $\times (\times 10^{11})$	Std $(\times 10^{11})$	Ranges (10^{-3})
E_1^c (Pa)	Log-normal	2.1	0.1	–
E_2^c (Pa)	Log-normal	2.1	0.1	–
E_3^c (Pa)	Log-normal	$\mu_{E3} \in [1.5, 2.5]$	$\sigma_{E3} \in [0.15, 0.25]$	–
E_4^c (Pa)	Log-normal	$\mu_{E4} \in [1.5, 2.5]$	$\sigma_{E4} \in [0.15, 0.25]$	–
A_1^c (m ²)	–	–	–	[7,8]
A_2^c (m ²)	–	–	–	[7,8]
A_3^c (m ²)	–	–	–	[7,8]
A_4^c (m ²)	–	–	–	[7,8]

are displayed in Table 8 accompanying with the reference values obtained by the same double-loop scheme as above. As shown in Table 8, the estimates of the bounds of failure probability evaluated by are consistent with the reference bounds. The optimal points of CABO show no difference with the reference points. In summary, the CABO method can well estimate the bounds of variance and failure probability with high accuracy and efficiency.

Table 7: Results for bounds of response variance of the transmission tower.

Method	Bounds	Means	Optima of \mathbf{x}_{III} and $\boldsymbol{\theta}$	Posterior COVs (%)	N_{call}
Reference	Lower	1.1320	(0.008,0.008,0.008,0.008) (2.5, 2.5, 0.15, 0.15) $\times 10^{11}$	–	–
	Upper	2.6431	(0.007, 0.007, 0.007, 0.007) (1.5, 1.5, 0.25, 0.25) $\times 10^{11}$	–	–
CABO	Lower	1.269	(0.0074,0.0073,0.008,0.008) (2.5, 2.27, 0.23, 0.246) $\times 10^{11}$	0.41	25+6+20=51
	Upper	2.605	(0.007, 0.008, 0.0075, 0.007) (1.5, 1.5, 0.25, 0.15) $\times 10^{11}$	0.24	–

Table 8: Results for bounds of failure probability of the transmission tower.

Method	Bounds	Means	Optima of \mathbf{x}_{III} and $\boldsymbol{\theta}$	Posterior COVs (%)	N_{call}
Reference	Lower	0	(0.007, 0.008, 0.007, 0.007) (2.5, 2.5, 2.07, 0.25) $\times 10^{11}$	–	–
	Upper	0.0736	(0.008, 0.008, 0.008, 0.008) (2.5, 2.5, 0.249, 0.25) $\times 10^{11}$	–	–
CABO	Lower	0	(0.0077, 0.0079, 0.0074, 0.0074) (1.74, 1.67, 0.18, 0.23) $\times 10^{11}$	–	30+0+13=43
	Upper	0.0765	(0.008, 0.008, 0.008, 0.008) (2.5, 2.5, 0.25, 0.25) $\times 10^{11}$	0.06	–

5.4. Dynamic analysis of satellite

Consider a satellite(see Ref.[59]) whose FE model is displayed in Figure 7. The main structure of the satellite is a cubic core reinforced by the internal stiffening beams, and reflectors and photovoltaic are connected to the core by connecting beams. The corresponding FE model is composed of beam and

shell elements with 1262 elements and 7146 degrees-of-freedom. Assume that the Young's modulus of different components of the satellite are non-deterministic variables and modeled by different uncertainty characteristic models, and the specific distributional information of which is given in Table 9. Following the notations given in section 2, we have $\mathbf{x}_I = (E_1, E_2)$, $x_{II} = E_3$, $\mathbf{x}_{III} = (E_4, E_5)$ and $\boldsymbol{\theta} = (\mu_{E3}, \sigma_{E3})$. For this satellite structure, the first natural frequency of satellite plays an important role in reliability analysis, therefore, we assume that, the satellite will fail when the first natural frequency is less than a given threshold, the limit state function of the satellite is formulated as:

$$g(\mathbf{x}) = d_A(\mathbf{x}) - 1.794 \quad (43)$$

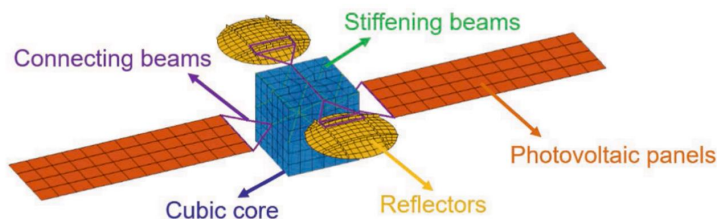


Figure 7: The geometric structure and environmental condition of the transmission tower.

Table 9: The distributional information of Young's modulus of the satellite.

Parameters	Distribution type	Means	Std	Ranges
E_1 (cubic core,Pa)	Log-normal	6.89×10^9	3.49×10^8	–
E_2 (photovoltaic panels,Pa)	Log-normal	6.89×10^9	3.49×10^8	–
E_3 (reflectors,Pa)	Log-normal	$\mu_{E3} \in [6.4, 9.6] \times 10^{10}$	$\sigma_{E3} \in [0.4, 0.8] \times 10^{10}$	–
E_4 (connecting beams,Pa)	–	–	–	$[6.4, 9.6] \times 10^{10}$
E_5 (stiffening beams,Pa)	–	–	–	$[6.4, 9.6] \times 10^{11}$

To estimate the bounds of the response variance, let the value of N_0 be 30, the sample size N_x of \mathbf{W} be 10^4 , the sample size N_g of the GPR model be 10^3 , the stopping threshold Δ^{BO} be 0.001 and Δ^{PVC} be 0.01. With the above settings, the results of CABO are shown in Table 10. The results displayed in Table 10 indicate that the estimates of bounds are accurate and reliable as the COVs are adequately small. By using the procedure of evaluating the bounds of variance, the estimates of bounds of failure probability are given in Table 10. It also can be observed that the upper bounds are accurately approximated by 0.0064 with COV being 0.06.

6. Conclusions

We conclude the developments and main findings in this section. As has been reported, an efficient framework named as CABO is proposed to estimate the bounds of variance and failure probability of

Table 10: Results of response variance and failure probability bounds for the satellite estimated by CABO.

Objective	Bounds	Means	Optima of \mathbf{x}_{III} and $\boldsymbol{\theta}$	COVs (%)	N_{call}
Variance	Lower	4.87×10^{-5}	$(6.4 \times 10^{10}, 6.4 \times 10^{11})$ $(7.703 \times 10^{10}, 0.04 \times 10^{10})$	$< 10^{-4}$	30+4+2=36
	Upper	19.079×10^{-5}	$(9.6 \times 10^{10}, 6.621 \times 10^{11})$ $(9.6 \times 10^{10}, 0.08 \times 10^{10})$	$< 10^{-4}$	
Failure probability	Lower	0	$(7.079 \times 10^{10}, 8.4748 \times 10^{11})$ $(7.085 \times 10^{10}, 0.0429 \times 10^{10})$	–	30+0+10=40
	Upper	0.0064	$(6.4 \times 10^{10}, 6.8115 \times 10^{11})$ $(6.4 \times 10^{10}, 0.0598 \times 10^{10})$	$< 10^{-4}$	

an engineering structure with three categories of non-deterministic inputs variables, i.e. precise random variables, imprecise random variables, and interval variables, where the imprecise random variables are modeled by a parameterized p-box. Before applying the procedure of CABO, it is necessary to transform the imprecise random variables to independent uniform distributional inputs and interval epistemic parameters, then the variance and failure probability are functions of interval variables and interval epistemic parameters. The BO and BC are then implemented in a collaborative and adaptive way by updating the GPR model in the augmented space of aleatory and epistemic uncertainties. Specifically, the BO equipped with the EI acquisition function is implemented in the marginal space of epistemic uncertainties for searching the global optima, and the BC equipped with PVC or U acquisition functions is jointly implemented for inferring the posterior distribution of the response variance and failure probability at deterministic sites specified by BO. The above two steps produce a new training point in the augmented space until both stopping conditions for BO and BC are satisfied. Benefiting from the collaborative learning scheme, the CABO algorithm requires only one simulator call for each iteration, making the algorithm especially efficient.

Benefiting from the collaborative and active learning scheme in the augmented space, the CABO algorithm has several superiority. First, the double-loop curse is completely broken, making the computation of bounds of any probabilistic descriptors (e.g., response variance and failure probability) efficient. Second, the global convergence of the EI function, which was theoretically proved in Refs. [60, 61], has been inherited by the CABO algorithm. Third, the CABO algorithm is gradient-free, thus does not require any extra numerical effort for computing gradients. For sure, nothing is given without a disadvantage in it. Due to the necessity of active learning in the augmented space, the GPR model needs to be trained in the $(n_I + n_{II} + n_{III} + n_\theta)$ -dimensional space, which limits the applicability of the CABO algorithm to high-dimensional problems with e.g., $n_I + n_{II} + n_{III} + n_\theta > 30$. This limitation can be further overcome by introducing some built-in dimensional reduction techniques (see e.g., Ref. [62]). This is a general issue for training the GPR model, and we don't present more details. Besides, the performance of the CABO algorithm largely depends on the utilized acquisition functions, and this work open the door for designing more effective acquisition functions with better trade-off between exploration and exploitation.

The results of benchmark studies show that, for all examples, the bounds for both response variance and failure probability are accurately and robustly estimated with high efficiency even when the input epistemic uncertainty is large. It is also noted from the results that, in case that the bounds of failure probability are very small values (typically less than 10^{-3}), the MCS procedure embedded in CABO may not be appropriate due to the large variation of estimates, and advanced MCS procedures, such as subset simulation and line sampling need to be properly integrated into the CABO framework. This will be treated in future work.

Acknowledgment

This work is supported by the National Natural Science Foundation of China under grant number 72171194 and 12202358, as well as the Sino-German Mobility Programme under grant number M-0175 (2021-2023).

Data availability

The codes are available upon request to the corresponding author.

Declaration of interests

The authors declare that they have no known competing financial interests or personal relationships that could have appeared to influence the work reported in this paper.

References

- [1] S. Zein, A. Laurent, D. Dumas, Simulation of a gaussian random field over a 3D surface for the uncertainty quantification in the composite structures, *Computational Mechanics* 63 (6) (2019) 1083–1090.
- [2] C. Ding, R. R. Deokar, X. Cui, G. Li, Y. Cai, K. K. Tamma, Proper orthogonal decomposition and Monte carlo based isogeometric stochastic method for material, geometric and force multi-dimensional uncertainties, *Computational Mechanics* 63 (3) (2019) 521–533.
- [3] A. Der Kiureghian, O. Ditlevsen, Aleatory or epistemic? does it matter?, *Structural Safety* 31 (2) (2009) 105–112.
- [4] M. Abdar, F. Pourpanah, S. Hussain, D. Rezazadegan, L. Liu, M. Ghavamzadeh, P. Fieguth, X. Cao, A. Khosravi, U. R. Acharya, et al., A review of uncertainty quantification in deep learning: Techniques, applications and challenges, *Information Fusion* 76 (2021) 243–297.
- [5] M. Beer, S. Ferson, V. Kreinovich, Imprecise probabilities in engineering analyses, *Mechanical Systems and Signal Processing* 37 (1-2) (2013) 4–29.
- [6] L. G. Crespo, S. P. Kenny, D. P. Giesy, Reliability analysis of polynomial systems subject to p-box uncertainties, *Mechanical Systems and Signal Processing* 37 (1-2) (2013) 121–136.
- [7] H. Agarwal, J. E. Renaud, E. L. Preston, D. Padmanabhan, Uncertainty quantification using evidence theory in multidisciplinary design optimization, *Reliability Engineering & System Safety* 85 (1-3) (2004) 281–294.
- [8] S. Sankararaman, S. Mahadevan, Distribution type uncertainty due to sparse and imprecise data, *Mechanical Systems and Signal Processing* 37 (1-2) (2013) 182–198.
- [9] J. C. Helton, J. D. Johnson, W. L. Oberkampf, C. J. Sallaberry, Representation of analysis results involving aleatory and epistemic uncertainty, *International Journal of General Systems* 39 (6) (2010) 605–646.
- [10] M. Faes, D. Moens, Recent trends in the modeling and quantification of non-probabilistic uncertainty, *Archives of Computational Methods in Engineering* (2019) 1–39.
- [11] L. G. Crespo, S. P. Kenny, D. P. Giesy, The nasa langley multidisciplinary uncertainty quantification challenge, in: 16th AIAA Non-Deterministic Approaches Conference, 2014, p. 1347.

- [12] P. Wei, J. Song, S. Bi, M. Broggi, M. Beer, Z. Lu, Z. Yue, Non-intrusive stochastic analysis with parameterized imprecise probability models: I. performance estimation, *Mechanical Systems and Signal Processing* 124 (2019) 349–368.
- [13] I. Behmanesh, B. Moaveni, G. Lombaert, C. Papadimitriou, Hierarchical Bayesian model updating for structural identification, *Mechanical Systems and Signal Processing* 64 (2015) 360–376.
- [14] P. Wei, F. Hong, K.-K. Phoon, M. Beer, Bounds optimization of model response moments: a twin-engine Bayesian active learning method, *Computational Mechanics* 67 (5) (2021) 1273–1292.
- [15] A. Tabandeh, N. Sharma, P. Gardoni, Uncertainty propagation in risk and resilience analysis of hierarchical systems, *Reliability Engineering & System Safety* 219 (2022) 108208.
- [16] X. Guo, J. Ji, F. Khan, L. Ding, Q. Tong, A novel fuzzy dynamic Bayesian network for dynamic risk assessment and uncertainty propagation quantification in uncertainty environment, *Safety science* 141 (2021) 105285.
- [17] M. de Angelis, E. Patelli, M. Beer, Advanced line sampling for efficient robust reliability analysis, *Structural Safety* 52 (2015) 170–182.
- [18] N. Pedroni, E. Zio, Hybrid uncertainty and sensitivity analysis of the model of a twin-jet aircraft, *Journal of Aerospace Information Systems* 12 (1) (2015) 73–96.
- [19] H. Zhang, R. L. Mullen, R. L. Muhanna, Interval Monte carlo methods for structural reliability, *Structural Safety* 32 (3) (2010) 183–190.
- [20] H. Zhang, H. Dai, M. Beer, W. Wang, Structural reliability analysis on the basis of small samples: an interval quasi-Monte carlo method, *Mechanical Systems and Signal Processing* 37 (1-2) (2013) 137–151.
- [21] D. A. Alvarez, F. Uribe, J. E. Hurtado, Estimation of the lower and upper bounds on the probability of failure using subset simulation and random set theory, *Mechanical Systems and Signal Processing* 100 (2018) 782–801.
- [22] E. Patelli, D. A. Alvarez, M. Broggi, M. d. Angelis, Uncertainty management in multidisciplinary design of critical safety systems, *Journal of Aerospace Information Systems* 12 (1) (2015) 140–169.
- [23] P. Wei, Z. Lu, J. Song, Extended Monte carlo simulation for parametric global sensitivity analysis and optimization, *AIAA journal* 52 (4) (2014) 867–878.
- [24] J. Song, P. Wei, M. Valdebenito, S. Bi, M. Broggi, M. Beer, Z. Lei, Generalization of non-intrusive imprecise stochastic simulation for mixed uncertain variables, *Mechanical Systems and Signal Processing* 134 (2019) 106316.
- [25] M. G. Faes, M. A. Valdebenito, D. Moens, M. Beer, Bounding the first excursion probability of linear structures subjected to imprecise stochastic loading, *Computers & Structures* 239 (2020) 106320.
- [26] M. G. Faes, M. A. Valdebenito, D. Moens, M. Beer, Operator norm theory as an efficient tool to propagate hybrid uncertainties and calculate imprecise probabilities, *Mechanical Systems and Signal Processing* 152 (2021) 107482.
- [27] P. Ni, D. J. Jerez, V. C. Fragkoulis, M. G. Faes, M. A. Valdebenito, M. Beer, Operator norm-based statistical linearization to bound the first excursion probability of nonlinear structures subjected to imprecise stochastic loading, *ASCE-ASME Journal of Risk and Uncertainty in Engineering Systems, Part A: Civil Engineering* 8 (1) (2022) 04021086.
- [28] M. Fina, C. Lauff, M. G. Faes, M. A. Valdebenito, W. Wagner, S. Freitag, Bounding imprecise failure probabilities in structural mechanics based on maximum standard deviation, *Structural Safety* 101 (2023) 102293.
- [29] P. Wei, J. Song, S. Bi, M. Broggi, M. Beer, Z. Lu, Z. Yue, Non-intrusive stochastic analysis with parameterized imprecise probability models: II. reliability and rare events analysis, *Mechanical Systems and Signal Processing* 126 (2019) 227–247.
- [30] M. Kitahara, J. Song, P. Wei, M. Broggi, M. Beer, A distributionally robust approach for mixed aleatory and epistemic uncertainties propagation, *AIAA Journal* (2022) 1–7.
- [31] J. Song, M. Valdebenito, P. Wei, M. Beer, Z. Lu, Non-intrusive imprecise stochastic simulation by line sampling, *Structural Safety* 84 (2020) 101936.
- [32] J. Fox, G. Okten, Polynomial chaos as a control variate method, *SIAM Journal on Scientific Computing* 43 (3) (2021) A2268–A2294.
- [33] O. I. Abiodun, A. Jantan, A. E. Omolara, K. V. Dada, N. A. Mohamed, H. Arshad, State-of-the-art in artificial neural network applications: A survey, *Heliyon* 4 (11) (2018) e00938.
- [34] C. E. Rasmussen, C. Williams, *Gaussian processes for machine learning*, vol. 1, MIT press 39 (2006) 40–43.
- [35] P. Wei, F. Liu, M. Valdebenito, M. Beer, Bayesian probabilistic propagation of imprecise probabilities with large epistemic uncertainty, *Mechanical Systems and Signal Processing* 149 (2021) 107219.
- [36] P. Hennig, M. A. Osborne, M. Girolami, Probabilistic numerics and uncertainty in computations, *Proceedings of the Royal Society A: Mathematical, Physical and Engineering Sciences* 471 (2179) (2015) 20150142.
- [37] P. I. Frazier, A tutorial on Bayesian optimization, *arXiv preprint arXiv:1807.02811* (2018).
- [38] F.-X. Briol, C. J. Oates, M. Girolami, M. A. Osborne, D. Sejdinovic, et al., Probabilistic integration: A role in statistical computation?, *Statistical Science* 34 (1) (2019) 1–22.
- [39] P. Wei, Y. Zheng, J. Fu, Y. Xu, W. Gao, An expected integrated error reduction function for accelerating Bayesian active learning of failure probability, *Reliability Engineering & System Safety* 231 (2023) 108971.
- [40] P. Hennig, M. A. Osborne, H. P. Kersting, *Probabilistic Numerics: Computation as Machine Learning*, Cambridge University Press, 2022.
- [41] L. Le Gratiet, C. Cannamela, B. Iooss, A Bayesian approach for global sensitivity analysis of (multifidelity) computer codes, *SIAM/ASA Journal on Uncertainty Quantification* 2 (1) (2014) 336–363.
- [42] C.-C. Li, A. Der Kiureghian, Optimal discretization of random fields, *Journal of engineering mechanics* 119 (6) (1993) 1136–1154.
- [43] S. Huang, S. Mahadevan, R. Rebba, Collocation-based stochastic finite element analysis for random field problems, *Probabilistic engineering mechanics* 22 (2) (2007) 194–205.
- [44] J. Chen, W. Sun, J. Li, J. Xu, Stochastic harmonic function representation of stochastic processes, *Journal of Applied Mechanics* 80 (1) (2013).

- [45] J. Wilson, V. Borovitskiy, A. Terenin, P. Mostowsky, M. Deisenroth, Efficiently sampling functions from gaussian process posteriors, in: International Conference on Machine Learning, PMLR, 2020, pp. 10292–10302.
- [46] S. Vakili, H. Moss, A. Artemev, V. Dutordoir, V. Picheny, Scalable thompson sampling using sparse gaussian process models, *Advances in Neural Information Processing Systems* 34 (2021) 5631–5643.
- [47] S. Huang, S. Quek, K. Phoon, Convergence study of the truncated Karhunen–Loève expansion for simulation of stochastic processes, *International journal for numerical methods in engineering* 52 (9) (2001) 1029–1043.
- [48] J. Wu, X.-Y. Chen, H. Zhang, L.-D. Xiong, H. Lei, S.-H. Deng, Hyperparameter optimization for machine learning models based on Bayesian optimization, *Journal of Electronic Science and Technology* 17 (1) (2019) 26–40.
- [49] D. Zhan, H. Xing, Expected improvement for expensive optimization: a review, *Journal of Global Optimization* 78 (3) (2020) 507–544.
- [50] J. Wu, P. Frazier, The parallel knowledge gradient method for batch Bayesian optimization, *Advances in neural information processing systems* 29 (2016).
- [51] J. M. Hernández-Lobato, M. W. Hoffman, Z. Ghahramani, Predictive entropy search for efficient global optimization of black-box functions, *Advances in neural information processing systems* 27 (2014).
- [52] P. Wei, X. Zhang, M. Beer, Adaptive experiment design for probabilistic integration, *Computer Methods in Applied Mechanics and Engineering* 365 (2020) 113035.
- [53] J. Song, P. Wei, M. A. Valdebenito, M. Faes, M. Beer, Data-driven and active learning of variance-based sensitivity indices with Bayesian probabilistic integration, *Mechanical Systems and Signal Processing* 163 (2022) 108106.
- [54] B. Echard, N. Gayton, M. Lemaire, AK-MCS: an active learning reliability method combining Kriging and Monte carlo simulation, *Structural Safety* 33 (2) (2011) 145–154.
- [55] B. J. Bichon, M. Eldred, L. P. Swiler, S. Mahadevan, J. M. McFarland, Efficient global reliability analysis for nonlinear implicit performance functions, *AIAA Journal* 46 (2008) 2459–2468.
- [56] Z. Lv, Z. Lu, P. Wang, A new learning function for Kriging and its applications to solve reliability problems in engineering, *Computers & Mathematics with Applications* 70 (5) (2015) 1182–1197.
- [57] K. Yan, Y. Wu, B. Zhang, Z. Zhong, Probability based method for attitude control system parameters design of space vehicle, *Flight Dynamics* 39 (1) (2021) 88–94.
- [58] T. Haukaas, A. Der Kiureghian, Strategies for finding the design point in non-linear finite element reliability analysis, *Probabilistic Engineering Mechanics* 21 (2) (2006) 133–147.
- [59] T. Abrahamsson, D. Kammer, Finite element model calibration using frequency responses with damping equalization, *Mechanical systems and signal processing* 62 (2015) 218–234.
- [60] E. Vazquez, J. Bect, Convergence properties of the expected improvement algorithm with fixed mean and covariance functions, *Journal of Statistical Planning and inference* 140 (11) (2010) 3088–3095.
- [61] A. D. Bull, Convergence rates of efficient global optimization algorithms., *Journal of Machine Learning Research* 12 (10) (2011) 2879–2904.
- [62] R. Tripathy, I. Bilionis, M. Gonzalez, Gaussian processes with built-in dimensionality reduction: Applications to high-dimensional uncertainty propagation, *Journal of Computational Physics* 321 (2016) 191–223.